

LA-UR-83-210

Los Alamos National Laboratory is operated by the University of California for the United States Department of Energy under contract W-7405-ENG-36.

## OFFSET WELL TEST

A Field Tracer Experiment In Devonian  
Shale — Data, Qualitative Interpretations,  
And Preliminary Modeling

Los Alamos Los Alamos National Laboratory  
Los Alamos, New Mexico 87545

LA-UR-83-210

Issued: January 1983

## **OFFSET WELL TEST**

# **A Field Tracer Experiment In Devonian Shale — Data, Qualitative Interpretations, And Preliminary Modeling**

Thomas L. Cook

Lee F. Brown

Wayne R. Meadows

Bryan J. Travis

## TABLE OF CONTENTS

Acknowledgments . . . . .	5
Abstract . . . . .	6
I. Executive Summary . . . . .	7
II. Introduction . . . . .	9
III. The Experiment . . . . .	12
A. Geology . . . . .	12
B. Configuration . . . . .	13
C. Experimental Procedure . . . . .	14
D. Instrumentation . . . . .	15
IV. Presentation of Data . . . . .	17
A. Overview . . . . .	17
B. Data from Well A . . . . .	18
C. Data from Well C . . . . .	19
D. Data from Well B . . . . .	22
V. Delay Time, Downhole Compositions, and Flow Rates . . . . .	24
A. The Theoretical Delay Time in Well C . . . . .	24
B. Measured Delay Times in Well C . . . . .	24
C. Flow Rates and Downhole Compositions in Well C . . . . .	26
D. Delay Time, Downhole Compositions, and Flow Rates in Well A . . . . .	27
E. Well B Flow Rate . . . . .	28
VI. Discussion . . . . .	29
A. Connectivity of Wells . . . . .	29
B. Nitrogen Flow in Fracture and Matrix . . . . .	30
VII. Theory . . . . .	32
A. Introduction . . . . .	32
B. One-Dimensional Diffusion Model . . . . .	33
C. Two-Dimensional Pore/Fracture Flow . . . . .	37
VIII. Conclusion . . . . .	40
XI. Recommendations for Future Tests . . . . .	41
References . . . . .	43

Appendixes

A. Modeling and Equation Derivation . . . . .	70
B. Pre-Test Simulations . . . . .	77
C. Field-Test Data . . . . .	94
D. Downhole Pressure Data . . . . .	130

Table I. Sources of Structure in Data . . . . .	44
---	----

List of Figures

1. Downhole Well Separation . . . . .	45
2. Downhole Pipe Configuration . . . . .	45
3. Los Alamos Tracer Flow Trailer . . . . .	46
4. Wellhead Pressures . . . . .	47
5. Effluent Tracer Concentrations at Wellheads . . . . .	48
6. Comparison of Pressures Measured Downhole and at Wellhead in Well A . . . . .	49
7. Wellhead Pressures and Tracer Concentrations in Well A . . . . .	50
8. Wellhead Pressures and Tracer Concentrations in Well A during 100 psig Phase . . . . .	51
9. Concentrations of Methane and Ethane in Well A Effluent . . . . .	52
10. Methane/Ethane Ratio in Well A Effluent . . . . .	53
11. Wellhead Pressures and Tracer Concentrations in Well C Effluent . . . . .	54
12. Occurrences of Major Leaks in Well C . . . . .	55
13. Concentrations of Methane and Ethane in Well C Effluent . . . . .	56
14. Methane/Ethane Ratio and Nitrogen Percentage in Well C Effluent . . . . .	57
15. Comparison of Pressures Measured Downhole and at Wellhead in Well B . . . . .	58
16. Use of A and B Downhole Pressures to Indicate Delay Times Between Events in Wells . . . . .	59
17. Wellhead Pressures and Tracer Concentrations in Well B . . . . .	60
18. Concentrations of Methane and Ethane in Well B Effluent . . . . .	61

19.	Methane/Ethane Ratio and Nitrogen Percentage in Well B Effluent . .	62
20.	Time Lags Between Stops of the Leak in Well C and Falls in Effluent Tracer Content . . . . .	63
21.	Time Lags Between Starts of the Leak in Well C and Rises in Effluent Tracer Content . . . . .	64
22.	Occurrences of All Detectible Leaks in Well C . . . . .	65
23.	Wellhead Pressures and Downhole Tracer Concentrations in Well C . .	66
24.	Wellhead Pressures and Downhole Tracer Concentrations in Well A During 100 psig Phase . . . . .	67
25.	Measured Wellhead Pressures and Modeling Input for Well A . . . .	68
26.	Preliminary Modeling Results . . . . .	69
A1.	Penny-Shaped Fracture . . . . .	75
A2.	Calculational Cell in Cylindrical Geometry . . . . .	75
A3.	Cross-Sectional View of the Cylindrical Model . . . . .	76
B1.	Pre-Test Simulations; Base Case at 4 Days. . . . .	86
B2.	Pre-Test Simulations; Base Case at 11 Days. . . . .	87
B3.	Pre-Test Simulations; Well A Pressure and Concentration-Time Histories for the Base Case. . . . .	88
B4.	Pre-Test Simulations; Well C Pressure and Concentration-Time Histories for the Base Case. . . . .	89
B5.	Pre-Test Simulations; Pressure Patterns for the 4 Variations at 4 Days. . . . .	90
B6.	Pre-Test Simulations; Well C CH <sub>4</sub> Concentration-Time Histories for the 4 Variations. . . . .	91
B7.	Pre-Test Simulations; Well C N <sub>2</sub> Concentration-Time Histories for the 4 Variations. . . . .	92
B8.	Pre-Test Simulations; Well C CO <sub>2</sub> Concentration-Time Histories for the 4 Variations. . . . .	93

ACKNOWLEDGMENTS

The experiment described and discussed in this report could not have been carried out without the extensive and sincere help of many people, both from Los Alamos and elsewhere. Special thanks are expressed to Lincoln F. Elkins of Sohio Petroleum Company, who had the original concept of the experiment and talked about meanings of the resulting data; to Francis H. Harlow, who helped in refining the experimental approach and aided in the modeling; to Robert Lawton and Bert Dennis, who oversaw the equipping of the instrument trailer and programmed the computers in it; to Karl-Heinz Frohne of DOE's Morgantown Energy Technology Center, who gave technical support in both office and field; and to Robb Hermes and Kirk Binning, who helped calibrate the instruments and take the data.

ABSTRACT

To characterize Eastern Devonian gas shale, a seven-day tracer experiment was carried out in August, 1981, by the Los Alamos National Laboratory as part of the DOE's Offset Well Test. Two wells had been drilled in a Columbia Gas Company field in southeastern Ohio, each with a downhole separation of approximately 120 feet from an existing production well. The isosceles triangle formed by the three wells had an apex angle of approximately 110 degrees. The experiment was designed in pre-test studies by numerical simulation of gas flow in a porous medium interlaced throughout by an anisotropic fracture network (see Appendix B). The two-dimensional, multi-species TRACRKP code was used in these simulations. About 56,000 SCF of nitrogen were injected into a producing zone located 3300 ft deep in one of the wells. Gas was then produced from the various wells at different rates and pressures for the duration of the test. Pressure and effluent composition in the three wells were measured. The injected nitrogen dispersed throughout the formation, in spite of flow in the opposite direction (toward the injection well). There also was significant penetration of the shale matrix by the nitrogen. One-dimensional analysis of the pressure buildup and drawdown curves could not characterize the system adequately. Quantitative conclusions regarding the storage and transport characteristics of the region must await the completion of sophisticated TRACER calculations.

---

References, table, and illustrations at end of the main portion of report.

Work performed under the auspices of the US DOE, Morgantown Energy Technology Center. K.-H. Frohne, Technical Project Officer.

## I. EXECUTIVE SUMMARY

A tracer test can give details about downhole void structure, gas storage, and flow patterns which are available in no other fashion. This report presents the pre-test simulations, experimental results, and some preliminary interpretation from a tracer study carried out as part of the DOE's Offset Well Test (OWT). The tracer experiment used the three holes which were the focus of the OWT; the three wells formed a rough isosceles right triangle with an 18-year-old production well at the apex. The other two wells each were drilled approximately 120 ft from the production well for the OWT. Extensive pre-test two-dimensional TRACRKP-code simulations using the intended experimental plan were carried out. The simulations revealed flaws in the intended plan, and an alternative experimental strategy was developed (see Appendix B).

To start the field experiment, 56,000 SCF of nitrogen were injected into one of the new wells, called Well A. The gas was injected at a pressure of about 650 psig into a producing zone 3300 feet down. After the 9 3/4 hrs of injection, the pressure was decreased over a 1 1/2 hr period to 100 psig; the well was then back-produced for the next 135 hr at this pressure and at a flow rate of about 107 SCF/hr. Throughout the experiment, the old production well (Well C) had a flow of 80 SCF/hr except for rather frequent leaking periods. When Well C leaked, the flow was 390 SCF/hr. Well B, the other well drilled for the OWT, had a steady leak, and the flow rate was some undetermined value greater than 80 SCF/hr.

Pressure responses indicated a good connection between the nitrogen-injection well (Well A) and the old production well (Well C), but a poor connection between Well B and the other two. Well C's nitrogen-composition measurements confirmed the good connection between Wells A and C. Tracer results from Wells B and C showed that the nitrogen dispersed throughout the formation as the experiment progressed. This occurred in spite of the general flow in the direction of Well A, caused by the pressure in the injection well being kept below the pressures of Wells B and C. There also were indications of a stagnant region of higher nitrogen content very near Well C.

## II. INTRODUCTION

This report presents the results of the tracer-study portion of DOE's Offset Well Test. Two previous publications<sup>1,2</sup> described the experiment briefly, presented some of the data and made early analyses. Full details of the tracer study up to its present state are given here--the background, development of the experimental strategy, description of the experimental program, the resulting data, how the data were reduced to usable form, and the results of preliminary numerical analyses.

The efficient recovery of methane from Eastern gas shales awaits the implementation of improved stimulation techniques. Determination of the appropriate technique can be assisted by a better understanding of the methane storage and transport processes within the shale. Structurally, these Devonian shales consist of a low-porosity matrix interlaced throughout by a complex network of fractures, which are approximately perpendicular to the horizontal bedding planes. Although methane gas has been produced from Devonian shales in the Appalachian Basin for more than fifty years, there is still a wide divergence of opinion concerning the nature of the underground storage. Stimulation methods for production wells vary, depending on whether the methane is stored in the pores or in the fractures. Data collected during a tracer experiment in the DOE's Offset Well Test allows us to examine the relative proportion of storage in the pores and fractures.

The test was designed to determine not only the storage and transport properties of methane in Devonian shale but also to provide information regarding nominal fracture spacing and orientation in the deposit found in southeastern Ohio. To accomplish the latter objective, two new wells were drilled near an old methane well that continues to be a useful production well after eighteen years of flow. One of the new wells was offset from the old well in a direction believed to be parallel to the direction of the major regional fracture trend; the other, in a direction perpendicular to the trend. The original concept<sup>3</sup> for examining the storage characteristics of the shale, proposed by Lincoln F. Elkins of the SOHIO Petroleum Company,

back-produced the injection well. The old production well and the second new well were allowed to flow at a minimum rate of 80 SCF/hr for the entire test. Species-concentration and pressure data were collected at all three wells throughout the test. Details of the intended experimental plan and some field modifications of it are presented in Section III.C below.

The crucial rock characterization properties can only be surmized qualitatively from the field data alone. Detailed interpretations require matching the results from carefully formulated mathematical models of gas flow in fractured/porous media to these data. The rock is characterized by two basically different forms of porosity and permeability. One of these describes the potentially anisotropic and non-homogeneous network of fractures that interlaces about the unfractured blocks. The other describes the properties of the blocks themselves.

The fundamental structure of our models is based on the principles of mass and momentum conservation of a tracer-laden compressible gas flowing through a porous and permeable material. For each simulation a small number of parameters must be specified to characterize the rock. In part these can be measured by an analysis of samples from cores or outcrops. In part they must be derived by a careful comparison of calculated results with field-test data. When the data and calculated results match closely, then the parameters required for the matching calculations can be considered to characterize the rock properties. Moreover, the results of the matching calculation yield an abundance of information that is unavailable from field measurements.

When carried out for the Devonian shales under present consideration, the calculations show in detail the relative proportions of both methane and nitrogen (the injected tracer gas) in the fractures and the block pores as functions of both position and time. A detailed analysis of these results serves therefore to enhance greatly our knowledge about the methane storage and transport properties in the shale. From this analysis we can draw conclusions that permit a very concise characterization to be presented in a

layer contains a network of interconnected vertical fractures. For the Huron Member in Meigs County, where the test was performed, the highest frequency of parallel fractures has a N50°E to N60°E trend.<sup>6</sup>

B. Configuration:

Two wells were drilled near a producing methane well, which is officially registered as Well 10056. Well 10056 is referred to as Well C in the remainder of this report. Well A was offset from Well C in a direction parallel to the primary fracture trend described above. Well B was offset from Well C in a direction approximately perpendicular to the trend. Figure 1 shows the orientation and downhole separation of the three wells. The angle ACB is about 110° and the distances AC and CB are 118 ft.

Each of the new wells was drilled to a total depth of about 3500 ft, which is near the base of the Huron Member. The major gas producing zone lies in the interval 85-115 ft above the 3400 ft level in Wells A and C. From pressure buildup tests<sup>7</sup>, we conclude that Wells A and C are in closer communication than either is with Well B.

Figure 2 summarizes the pipe configuration in each well. Well C has a total depth of 3400 ft. The well is cased to a depth of 2120 ft and has a diameter of 7 in. Below this level the hole is uncased, having a nominal 6 1/4 in. diameter. The lower 200 ft of the well was shot loaded with nitroglycerin to enhance communication with the natural fracture network. Steel tubing having an inside diameter of 2.05 in. was inserted from the surface to a depth of 3400 ft. The lower 100 ft of the tubing is slotted to allow gas flow into the string. Figure 2b shows an enlarged view of the lower 170 ft of Well C. A downhole pressure package and supporting wire cable are also shown.

Wells A and B have 8 in. diameters and are cased to a depth of 2100 ft. The total depth of Well A is 3484 ft; of Well B, 3478 ft. A packer was set in Well A at a depth of 3315 ft, and tubing with an inside diameter of 2.05

locations throughout the test. The initial and boundary conditions were carefully monitored so that the introduction of possible ambiguities in the data could be minimized. It was felt that the unequivocal interpretation of the results required a continuous injection phase. That is, if injection (Phase 1) were interrupted, we would proceed immediately to back production (Phase 2). Supply arrangements permitted the uninterrupted injection of N<sub>2</sub> for 9-3/4 hrs at a constant wellhead pressure of 650 psig.

This pressure was selected because (1) it lay well below the virgin reservoir pressure before drilling (800 psi) and therefore would be unlikely to alter the existing fracture network, (2) it lay sufficiently above the shut-in pressure (400 psi) of the reservoir to force the tracer gas into the pore space if such a storage potential existed, and (3) it lay safely below the maximum pressure-differential constraints of the packer set in Well A to isolate the major gas-producing zone. Based on pressure and temperature data and on the respective N<sub>2</sub> tube trailer volumes, the total amount of N<sub>2</sub> injected was calculated to be 56,000 SCF.

#### D. Instrumentation

At the start of Phase 2, Well A was back-produced through a pressure regulator. After the pressure at the wellhead had dropped to 100 psig, the gas flow rate was adjusted throughout the remainder of the test to maintain this pressure. A small amount of gas (80 SCF/hr) was drawn off and run through the sampling lines of the Los Alamos instrument trailer. The experimental plan called for the flow at Wells C and B to be restricted to 80 SCF/hr. These boundary conditions were not realizable, because of a slow leak around a coupling near the base of the Well B christmas tree and because of a sporadically leaking rubber seal at Well C. A compressed N<sub>2</sub>-driven greaser was on location at Well C to prevent the leak, but the grease seal was breached several times during the test. From the data we have developed a log of this non-constant leak at Well C (see Section V).

The computer-controlled data collection system was housed in a Los

#### IV. PRESENTATION OF DATA

##### A. Overview

The wellhead pressures for the three wells throughout the test are presented in Fig. 4. The injection period is clearly visible in the Well A pressures, and it is followed by a very fast pressure drop to approximately 100 psig. There it remained for the rest of the experiment. Minor fluctuations in the pressure occurred during the 100-psig period, and the pressure was controlled manually by modifying the flow rate from the well.

The pressure in Well C (the old production well) rose steadily as nitrogen was injected, then fell as the injection well was back-produced. Significant fluctuations in Well C's pressure occurred sporadically, indicating the occurrence of the leak described earlier. The slow pressure rises resulted from re-sealing the well and temporarily eliminating the leak. The final drop in pressure occurred when the well was opened wide at the end of the test.

Well B's pressure trace shows a steady, though rather minor, rise throughout the duration of the experiment. A more precise analysis of the Well B pressure behavior will be presented below.

The percentages of the nitrogen tracer in the gases at the three wellheads are presented in Fig. 5. The injection phase in Well A is clearly marked by the high concentration of nitrogen. As this well was back-produced, the nitrogen content of the gas fell, decaying toward the background level. During the back-production phase, minor fluctuations occurred.

In Well C, the nitrogen composition began at a very low level, then surged three times, separated by periods of ten to seventeen hours. Following the first two surges, the nitrogen returned to the background concentration. After the third surge, the nitrogen remained at a significant

pressure and composition fluctuations more clearly. Qualitatively, it appears that an increase in the pressure fluctuations about the local mean might have been followed, some time later, by an increase in the fluctuations of the nitrogen composition about the local mean. A similar phenomenon is noted in the data from Well C, and the cause-and-effect relationship as well as conclusions from it are discussed below.

In addition to nitrogen, the effluent stream was also analyzed for methane and ethane content. Figure 9 shows the methane and ethane compositions in the Well A effluent over the period of the experiment. They appear to be effective mirrors of the nitrogen composition, being zero during the injection period, then rising slowly over the remainder of the test, with the rise approaching the steady-state composition value. The apparent ten-hour surges in both compositions, starting at about 70 hours, are ascribed to faulty calibrations during that time.

An interesting quantity is the ratio of methane to ethane amounts in the effluent gas, because it might indicate relative dispersion and diffusion parameters within different parts of the formation. In Fig. 10 this quantity is depicted, beginning at about 10 hr. Before this time, during the nitrogen injection phase, the numbers have no significance. At the end of the injection period, as the pressure fell, the methane-to-ethane ratio fell also. When the pressure leveled out, the ratio passed through a minimum, then rose over the next 20 hr to a value of approximately 9.5. It stayed there, with minor fluctuations, for the remainder of the test.

#### C. Data from Well C

Figure 11 is the equivalent, for Well C, of Fig. 7 -- it shows the wellhead pressure and nitrogen composition for Well C throughout the test. Both pressure and composition traces from this well exhibit significant structure.

At the beginning of the test, as nitrogen was being injected into Well

The first nitrogen surge in Well C has been ascribed to the injection of nitrogen into Well A, followed by a reversal of flow between Wells A and C. Table 1 shows that both the second and third surges were preceded by leaks. In Fig. 12 the second leak appears much more serious than the first one, which explains the higher amplitude of the third peak. The first leak was cured after one hour, the second only after three hours. The time lapse between the first leak and the second surge (10 hr) was greater than the lapse between the second leak and the third surge (4 hr). The leaks caused the flow in Well C to increase to an extent sufficient to draw gas from within the nitrogen front in the fracture network. The edge of the front would have been closer to Well C at the time of the second leak, and this could be one reason for the shorter time lapse between the second and the third nitrogen surges. The significant amount of nitrogen in the well effluent following the third surge is believed to originate from tracer which had spread throughout the formation.

The methane and ethane compositions of the Well C effluent are presented in Fig. 13. As in the case of Well A, they appear to mirror the nitrogen concentrations. The ten-hour span of poor calibration beginning at about 70 hours, noted in the Well A results (Fig. 9), can be seen here also.

The methane/ethane ratio in the Well A results appeared to be weakly correlated with the nitrogen content. In the Well C results (Fig. 14), the behavior of the methane/ethane ratio during the three nitrogen surges was very marked. When the nitrogen content was increasing, the methane/ethane ratio was low; when the nitrogen content was decreasing, the methane/ethane ratio is high. When the nitrogen level in the effluent was not changing significantly, whatever the level, then the methane/ethane ratio leveled off at about 9.6. It is difficult to determine whether this behavior was present later in the experiment, when the nitrogen which had spread into the formation was entering the well. Small late-time peaks are observable at 68, 92, and 115 hr, which are close to the times where the nitrogen concentrations took significant drops when the leaks were temporarily halted. However, these peaks are not much greater than the noise in the trace, and so

valve at the head of Well B was not opened until the beginning of the test. Sound indicated that the leak was in the vicinity of the Christmas tree at the head of Well B.

The pressure trace remained about level from the beginning of the test until the 28.2-hr point, when it began to rise again. This was evidently in response to the injection of nitrogen at high pressure in Well A, and the 28.2-hr lag between the injection and response again indicates the poor connectivity between Wells A and B.

Following a steady rise for about 56 hr, the pressure in Well B leveled off for the remainder of the test (the minor rise at about 100 hr occurred when the gage was removed and the clock rewound). The onset of this level period occurred 84.1 hr after the pressure in Well A was dropped to 100 psig and kept there. At the end of the test, when the valve at the head of Well B was closed, the pressure began to rise sharply because the leak was cured by the closing of the valve. The Amerada gage continued to indicate the rising pressure until removal.

Yet another indication of the poor connectivity between Well B and Wells A and C lies in the lag between the beginning of the rise in the Well A pressure at the -21 hr point and the corresponding rise in Well B's pressure, 21.8 hr later. The cause of the decrease and subsequent rise in Well A's pressure at this point is attributed to the onset of a leak in Well C and its cure. The 21.8-hr value of course is lower than the 26.4 and 28.2-hr lags mentioned above, and may be attributed to Well C being closer to Well B than Well A. For the two longer time lags, the instigating factors occurred in Well A (pressure increases), and for the shortest lag the source of the effect occurred in Well C (a leak and cure).

Figure 17 is the equivalent, for Well B, of Figs. 7 and 11--it shows the wellhead pressure and nitrogen composition for Well B throughout the test. A wave of nitrogen appeared at about 51 hr. The wave peaked at a

16.0, 12.3, and 12.3 hr. The last two delays had some indications of very brief leaks during the time lapses, and so the numbers are suspect. The values of 15.0 and 16.0 hr are therefore regarded as the most reliable of the four. Since the composition of the gas from Well C was being sampled once per hour at that time, the two values are in essential agreement. The average of these two values, 15.5 hr, is taken to have been the delay time when Well C was properly sealed.

One might have expected the leak rate to vary, depending on the manner in which the seal was breached. Consequently, the time lapses between the onsets of leaks and the subsequent rise in effluent nitrogen percentage would be expected to vary also. Figure 21 shows that this is not so. The time periods between the onset of a leak and the beginning of a rise in nitrogen content are 3.3, 3.0 or 5.0 (depending on interpretation of the data), 3.0, and 3.3 hr. Following this observation, an operator reported that the grease seal seemed to blow out in a plug when a leak occurred; if this were the normal occurrence, the leak rate would be the same almost every time the seal was breached. For analysis of the experiment, therefore, a delay time of 3.2 hr was chosen for the periods when the seal in Well C was leaking.

At the end of the experiment when the well was opened wide, only 0.8 hr passed between the time the well was opened and the rise of the effluent nitrogen content.

The pipe running the length of the well has been in service for eighteen years; undoubtedly corrosion products on the pipe wall have reduced the effective cross-sectional area of the pipe. For this to be the entire explanation of the difference between the 23 hr theoretical delay in Well C and the 15.5 hr actual delay, there would have had to be a 0.18 in. thick layer of corrosion deposits running the length of the pipe. This is not an unreasonable value, and is regarded as the probable cause of the difference between the theoretical and observed delays. Another possible contributor to the delay might have been a constant leak somewhere in the system between the rubber seal near the head of the well and the trailer, which was not noticed

downhole pressures in Well C were recorded; nevertheless, comparisons between wellhead and downhole pressures in the other two wells (Figs. 6 and 15) show that the differences between wellhead and downhole measurements were due principally to the hydrostatic head and the characteristics of both downhole and wellhead pressure traces were identical.

D. Delay Time, Downhole Compositions, and Flow Rates in Well A

In Well A, there was no indication of the type of leak that was sporadically present in Well C. During the period when the wellhead pressure of Well A was kept close to 100 psig, the flow rate was subject only to relatively minor modifications. As a reasonable approximation, therefore, the flow rate from Well A was considered constant. The time for gas to travel from the bottom to the top of the well was therefore also approximately constant. The result of this should be an ability to match the concentration changes in this well with the pressure changes by a simple shifting of the time axis of the concentration-time trace.

Figure 23 shows the final plot of a trial-and-error process to find the best match between the pressure changes and concentration changes. It resulted from the shifting of the time axis by 5.0 hr. In general, the match is quite good. Periods of very slight pressure change occur simultaneously with periods of very slight concentration change. Peaks in the pressure trace usually coincide with valleys in the concentration trace, and valleys in the pressure trace with peaks in the concentration trace. Some of the deviations from this general rule can be explained by a little higher or lower flow rate, combined with a little steeper pressure rise or fall, as in the pressure spike at the 92 hr point.

The pipe within Well A was put into place for the Offset Well Test and did not have the constrictive corrosion products presumed in Well C's pipe. With an i.d. of 2.05 in, at a mean pressure of 100 psig and a mean temperature of 85°F, a delay time of 5.0 hr would indicate a flow rate of 107 SCF/hr.

## VI. DISCUSSION

### A. Connectivity of Wells

There was a very good connection between Wells A and C. This is apparent both from the pressure traces and the downhole tracer composition in Well C. Before the injection of the nitrogen, the pressure in Well C was relatively steady at approximately 400 psig. Upon the injection of nitrogen into Well A, the pressure in Well C rose 2.5 psi during the first 20 min interval, 4.8 psi during the second, and continued rising steadily until first a leak in Well C and then the back-production of Well A stopped the pressure rise in Well C. Thus the pressure signal traveled with sufficient speed that its velocity was undetectable within the 20-min sampling intervals that were used.

The nitrogen composition in Well C responded with similar speed. A sampling point approximately 2 min after the start of nitrogen injection detected a slight rise in downhole tracer content. The rise of nitrogen percentage in Well C was not as steady as that of the pressure. The form of the rise (Fig. 23) may perhaps indicate that a change in downhole fracture structure occurred as the nitrogen was being injected, with one path closing and another being opened.

It was remarked earlier that there was poor connection between Well B and the other two wells. Whereas a pressure signal traveled very rapidly between Wells A and C, there were lapses of 22-28 hr between significant pressure rises in Wells A and C and the responses in Well B. When the pressure in Well A was dropped to a value in the vicinity of that in Well B, it was 84 hr before the effect of the drop was seen in Well B's behavior. A wave of nitrogen was detected at Well B, 50 hr after the injection into Well A began. All of these occurrences mean that the connections between the Well A - Well C fracture system and Well B are poor, although they do exist.

well annulus. The highs of 30%  $N_2$  in the second surge and 80% in the third indicate this. The two well flow rates are sufficiently close that such a stagnancy might have existed.

The change in composition with flow rates was exhibited in both Wells A and C, the former during the 100 psig period, the latter throughout the test. The data of Well A especially indicate that gas was flowing from both fracture and rock matrix. The gas in the matrix undoubtedly had less nitrogen than the gas in the fracture, and was less subject to the effects of total flow rate. Therefore a rise in nitrogen content should have occurred when the flow rate increased, and the nitrogen content should have fallen when the flow rate decreased. This is indeed what happened.

The data from Well C are not as definite in this instance because of the existence of the stagnant nitrogen pocket nearby. The later small surges may have stemmed from this source rather than the different amounts of flow from matrix and fracture.

Overall, flow within and from the matrix affected the results of this experiment markedly.

B. One-Dimensional Diffusion Model

We solve the simple one-dimensional diffusion equation used in most wellhead pressure-buildup and drawdown analyses.<sup>8,9</sup> The detailed derivation of this equation is included in Appendix A to identify specifically the assumptions inherent in such calculations. The failure of this model to represent the data adequately is discussed at the conclusion of this section. In cylindrical coordinates the equation is

$$\frac{\partial p}{\partial t} + \frac{1}{r} \frac{\partial}{\partial r} (p\bar{u}r) = 0 , \quad (1)$$

where  $p$  is the pressure,  $\bar{u}$ , the mean radial velocity,  $t$ , the time, and  $r$ , the radial distance from the center of the injection borehole.

It is useful to relate the fracture half-height,  $a$ , and the fracture spacing,  $w$ , to commonly measured average properties of the matrix. Two such quantities are the fracture porosity,  $\theta_f$ , and the fracture permeability,  $k_f$ . The fracture porosity is defined as the volume of the fractures divided by the total volume of the system,

$$\theta_f = \frac{2a}{w} . \quad (2)$$

The permeability is a measure of the resistance a medium offers to the flow of a fluid through it. In terms of the fracture half-height and spacing (Appendix A) we obtain,

$$k_f = \frac{2}{3} \frac{a^3}{w} \quad (3)$$

$$N = \frac{H\theta_f}{2a} \quad (8)$$

Substituting Eq. (8) into Eq. (6) we express the volume flow rate in terms of the surface area of the injection region and the fracture porosity,

$$\dot{V}(p) = 2\pi r_o H \theta_f \bar{u}_o \quad (9)$$

Equations (5) and (9) provide the basis for analyzing the data using this simple model. Because  $\mu$  is known, the pressure calculated at some distance  $r$  from Well A is a function of the ratio  $k_f/\theta_f$ . The time integral of Eq. (9) is the total volume of gas flowing into the network at pressure  $p$ . The temperature of the gas is very nearly constant; therefore, we obtain the total volume of gas injected at standard conditions from

$$V_s = \frac{p}{p_s} \int_0^{t_1} \dot{V}(p) dt \quad (10)$$

where  $V_s$  is the volume of the injected gas at standard conditions of temperature and pressure,  $p_s$ , and  $t_1$  is the duration of the injection phase. Equations (9) and (10) allow us to determine  $\theta_f$ . Because the ratio  $k_f/\theta_f$  is also known, we can calculate  $k_f$ .

The pressure-time history measured at Well A is shown for early time in Fig. 24. The pressure assumed for Well A in all calculations is represented by the circles and the dashed line in the figure. In the one-dimensional analyses, we attempt to match the pressure curve measured at Well C (Fig. 25) subject to the constraint imposed by the total quantity ( $1.6 \times 10^9$  cm<sup>3</sup> at STP) of N<sub>2</sub> injected.

proportionality constant  $\frac{dk}{dp}$  was assumed to be  $2.47 \times 10^{-20} \text{ cm}^2/\text{dyne/cm}^2$  for our model.

Although the value of  $\theta_f$  obtained above depends on several unknown quantities, principally  $r_o$  and  $H$ , we can nevertheless use it to estimate  $k_f$  from the  $k_f/\theta_f$  ratios indicated by the one-dimensional model. A very rough value would be  $1.6 \times 10^{-4}$  darcy for  $k_f$  in the direction of the major fracture trend. This procedure could be repeated for Well B, iterating back and forth to obtain a best fit to the pressure data in an average sense. The model could even be improved by allowing one-dimensional diffusion into the matrix. The assumptions involved in such an analysis are similar to those demonstrated above. There is no point in performing parametric fits to only part of the data set (the pressures), hence we turn now to a description of the two-dimensional phase of the analysis.

### C. Two-Dimensional Pore/Fracture Flow

The next stage of the modeling involves a significantly more complex representation of the geometry, geology, and physical processes. A family of TRACER computer codes has been developed in which the medium can be nonhomogeneous and anisotropic, and can consist of porous blocks interlaced throughout by a fracture network. In the code used here,<sup>4</sup> mechanical dispersion, adsorption, pressure-dependent permeability, and Forchheimer's correction to Darcy flow are included in the model, and five separate gas species can be followed. The general equation set considered is

$$\theta_i \frac{\partial \rho_j}{\partial \tau} + \nabla \cdot \rho_j \vec{u}_j = \nabla \cdot \theta_i \bar{D} \nabla \rho_j + \nabla \cdot \theta_i D_j^* \bar{\rho} \nabla C_j - \theta_i \rho_i K D_j \frac{\partial C_j}{\partial \tau}$$

$$u_i = - \frac{k_i \nabla p}{\bar{\mu} (1 + a \text{Re}_i)}, \quad \text{Re}_i = \frac{L_i \bar{\rho} |u_i|}{\bar{\mu}}, \quad \bar{\mu} = \mu(C_j, \mu_j) \quad (11)$$

that both  $k_p$  and  $\theta_p$  were too small. The applicability of this model has by no means been extensively investigated. The transport of two different species and even the effect of simple adsorption models can be investigated with it. We hope to complete this second step in the analysis and to proceed to the third and final stage as funding allows.

## IX. RECOMMNDATIONS FOR FUTURE TESTS

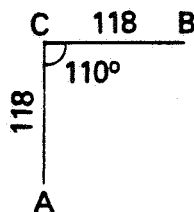
The pressure and flow fluctuations at Wells A and C gave important information. These were used to calculate flow and time-delay information, both of which are vital to the interpretation of the pressure- and concentration-time histories. Leaks will occur almost inevitably in any field test, and can render flow-meter data valueless. Thus the use of the results from sudden and minor pressure variations are necessary for the calculation of the true flows from the wells. In addition, the results of sudden and minor pressure variations appear to be the only means of determining the times required for the tracer to flow from the bottoms to the tops of the wells, and this is essential for calculating the downhole boundary conditions. Thus it is recommended that frequent, sudden, minor pressure variations be included in any experimental tracer study involving underground gas reservoirs.

The methane/ethane ratio was used to advantage in interpreting the test results. Since a known ratio of gases would give even more information, it is recommended that the possibility of injecting a known gas mixture be investigated in future pre-test simulations. Possible mixtures are  $N_2/CO_2$  and  $N_2^{13}CH_4$ . Each has advantages and drawbacks. The carbon dioxide is inexpensive, but its diffusional and adsorptive properties might render the results difficult to interpret. Carbon-13 is expensive, and analysis for the tagged methane would require a mass spectrometer. However, the flow of methane is the principal factor being investigated, and so the added expenses might be justified. Other possible mixtures should be considered.

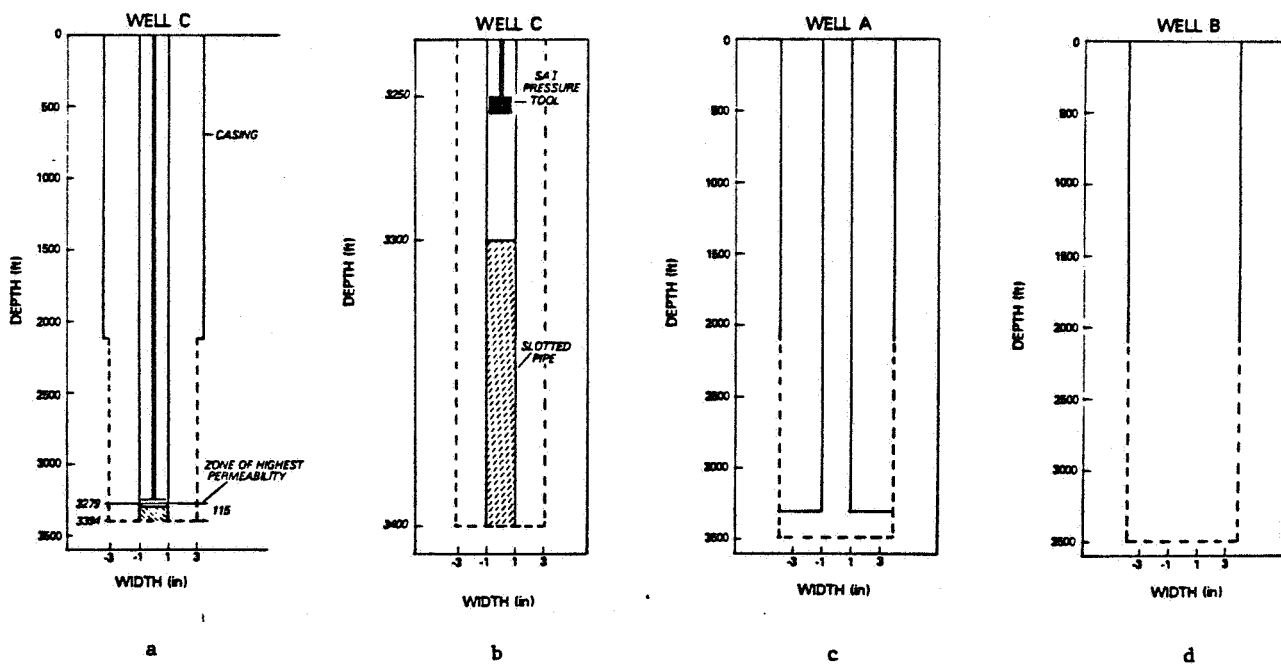
The pre-test simulations were critical to the success of this experiment. More extensive simulations unquestionably would have yielded an even better strategy for carrying out the experiment, especially if more knowledge of formation properties had been available. It is recommended that an assiduous effort be made to obtain as much information as possible concerning the formation, and that this be combined with more extensive

REFERENCES

1. Cook, T. L., Brown, L. F., and Meadows, W. R., "Tracer Experiments in Eastern Devonian Shale," paper # SPE 10707 of 1982 Unconventional Gas Recovery Symposium, Pittsburgh, PA, May 16-18 1982.
2. Cook, T. L., Brown, L. F., and Meadows, W. R., "Underground Flow Characteristics from a Field Tracer Experiment in Devonian Shale," Los Alamos National Laboratory report LA-UR-82-1344, Los Alamos, NM (1982).
3. Elkins, Lincoln F., "Determination of Fracture Void Volume in Devonian Shale Using Injection of Two Tracer Gases," Sohio Petroleum Company communication sent to Gulf Universities Research Consortium and to Gas Research Institute, Sept. 29, 1978.
4. Travis, B. J., "TRACRKP: Transient, Multicomponent, Two-Dimensional Flow in Porous/Fractured Media," Los Alamos National Laboratory, Los Alamos, NM (to be published, 1983).
5. Schwietering, Joseph F., "Devonian Shales of Ohio and Their Eastern and Southern Equivalents," Morgantown Energy Technology Center report METC/CR-79/2, January 1979, pp. 31-33.
6. Science Applications, Inc., Morgantown, West Virginia branch, "A Reservoir Engineering Study for the Offset Well Test Program," Final Report to Morgantown Energy Technology Center of DOE under Contract #DE-AM21-78MC08216, Task 23, December 19, 1980, p. 27.
7. Lee, B. O., Adam, J., Sawyer, W. L., Horan, K., and Frohne, K. H., "Evaluation of Devonian Shale Reservoir Using Multi-Well Pressure Transient Testing Data," paper # SPE 10738 of 1982 Unconventional Gas Recovery Symposium, Pittsburgh, PA, May 16-18, 1982.
8. Matthews, C. S., and Russell, D. G., "Pressure Buildup and Flow Tests in Wells," pp. 6, 10-12, 18 ff., 48 ff. AIME, Dallas, TX, 1967.
9. Earlougher, R. C., Jr., "Advances in Well Test Analysis," pp. 6-7. AIME, Dallas, TX, 1977.



Downhole Well Separation  
Figure 1



Downhole Pipe Configuration  
Figure 2

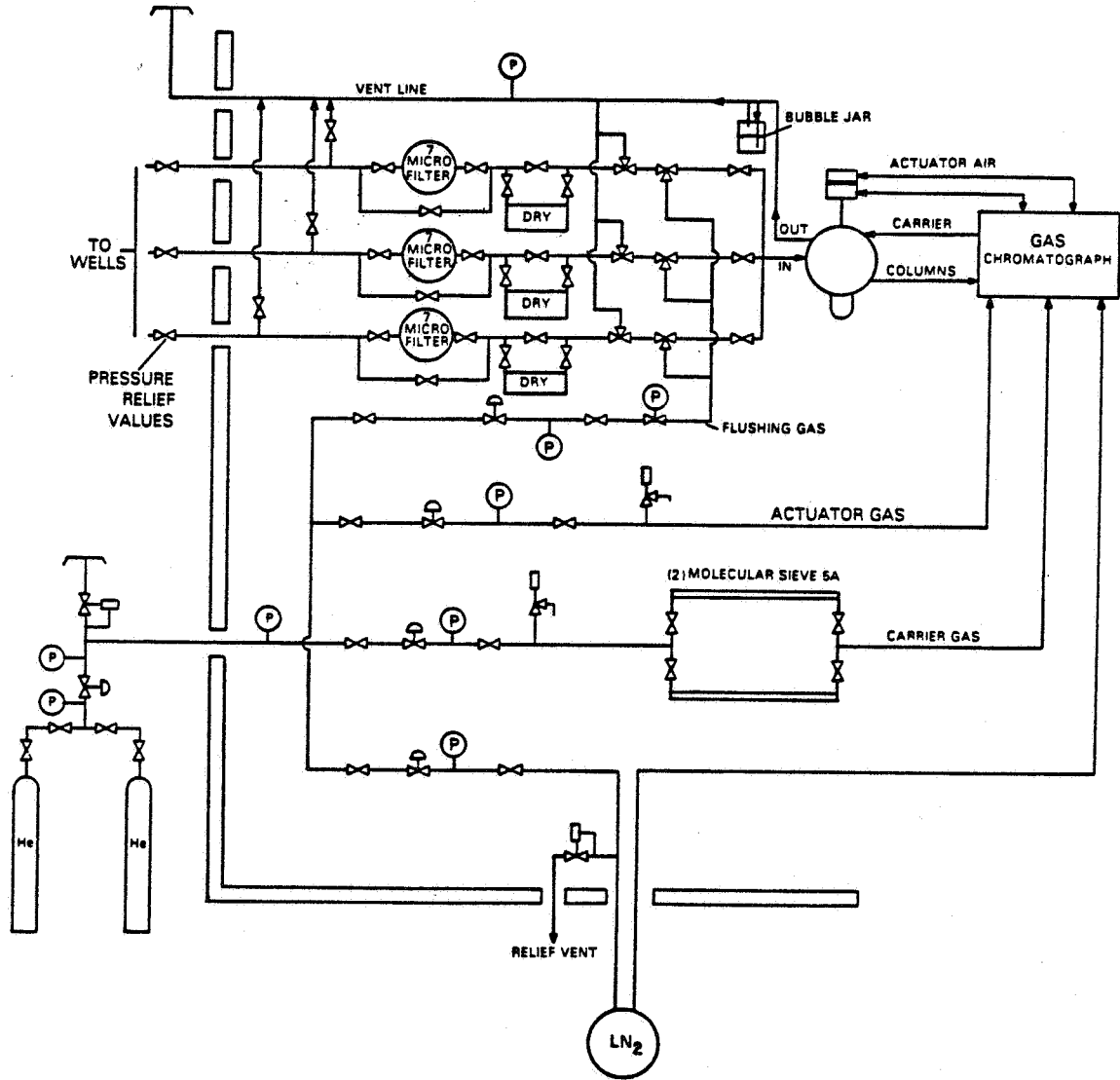
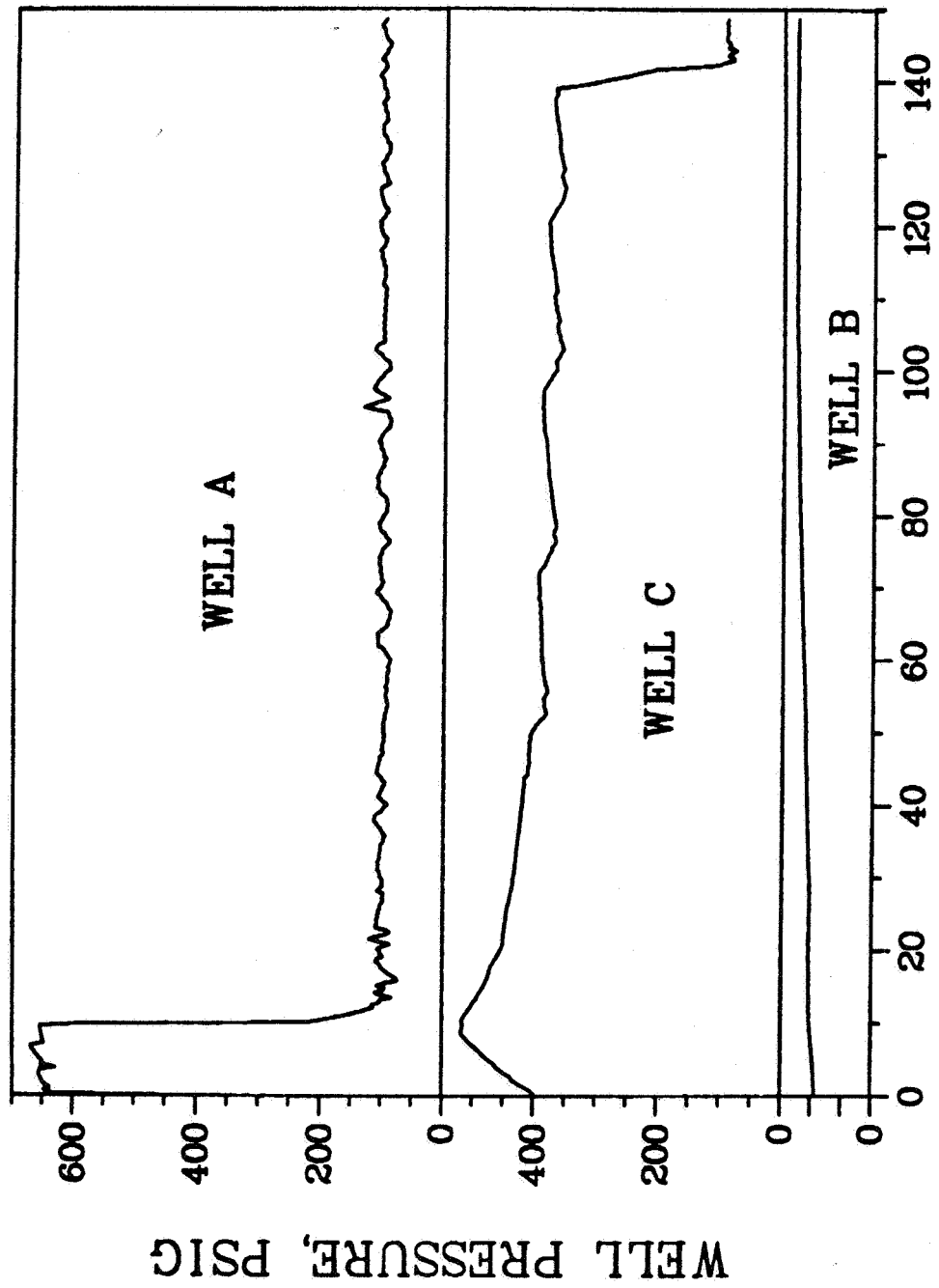


Figure 3. Los Alamos Tracer Flow Trailer



TIME ELAPSED IN TEST, HRS.

Figure 4. Wellhead Pressures

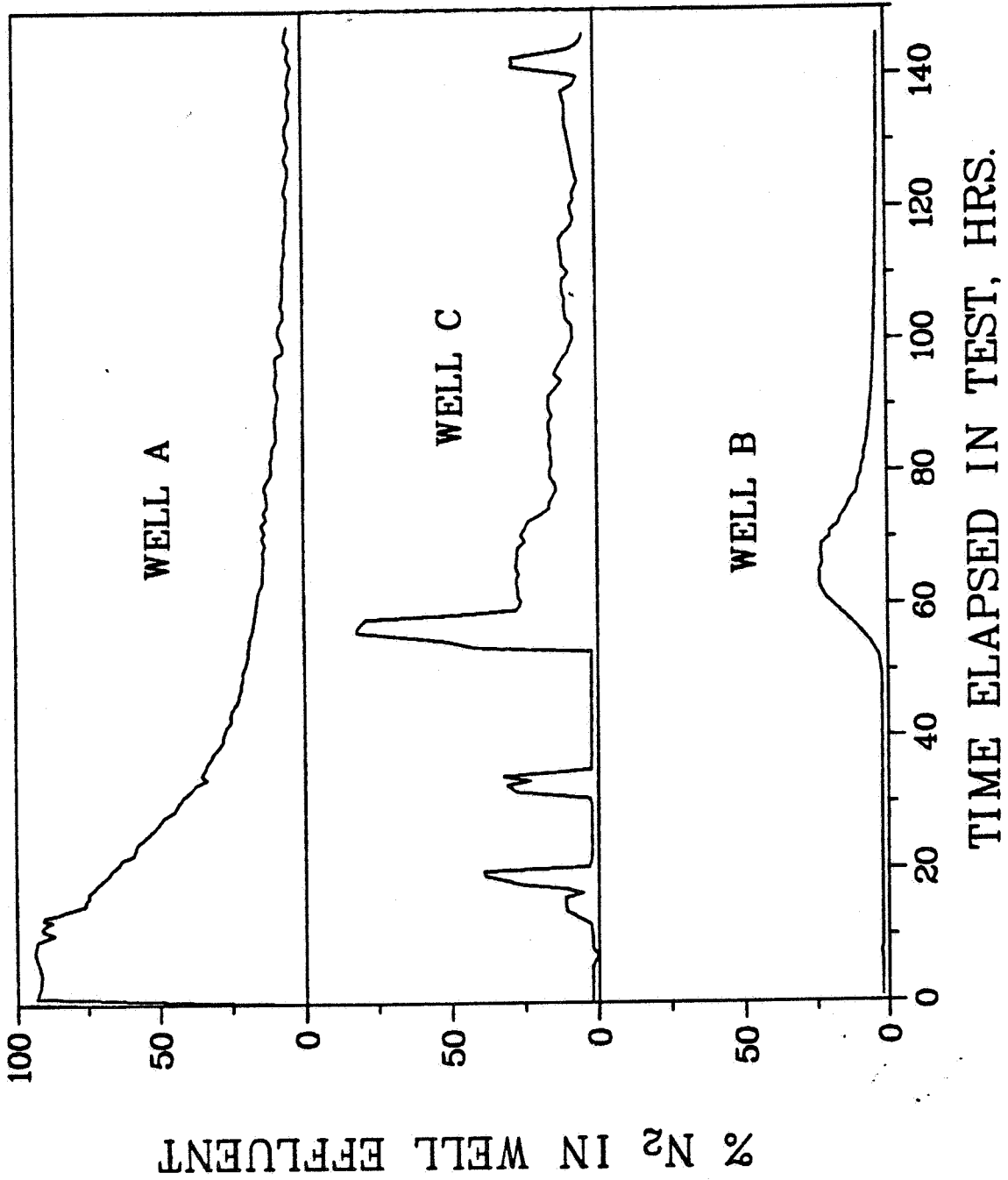
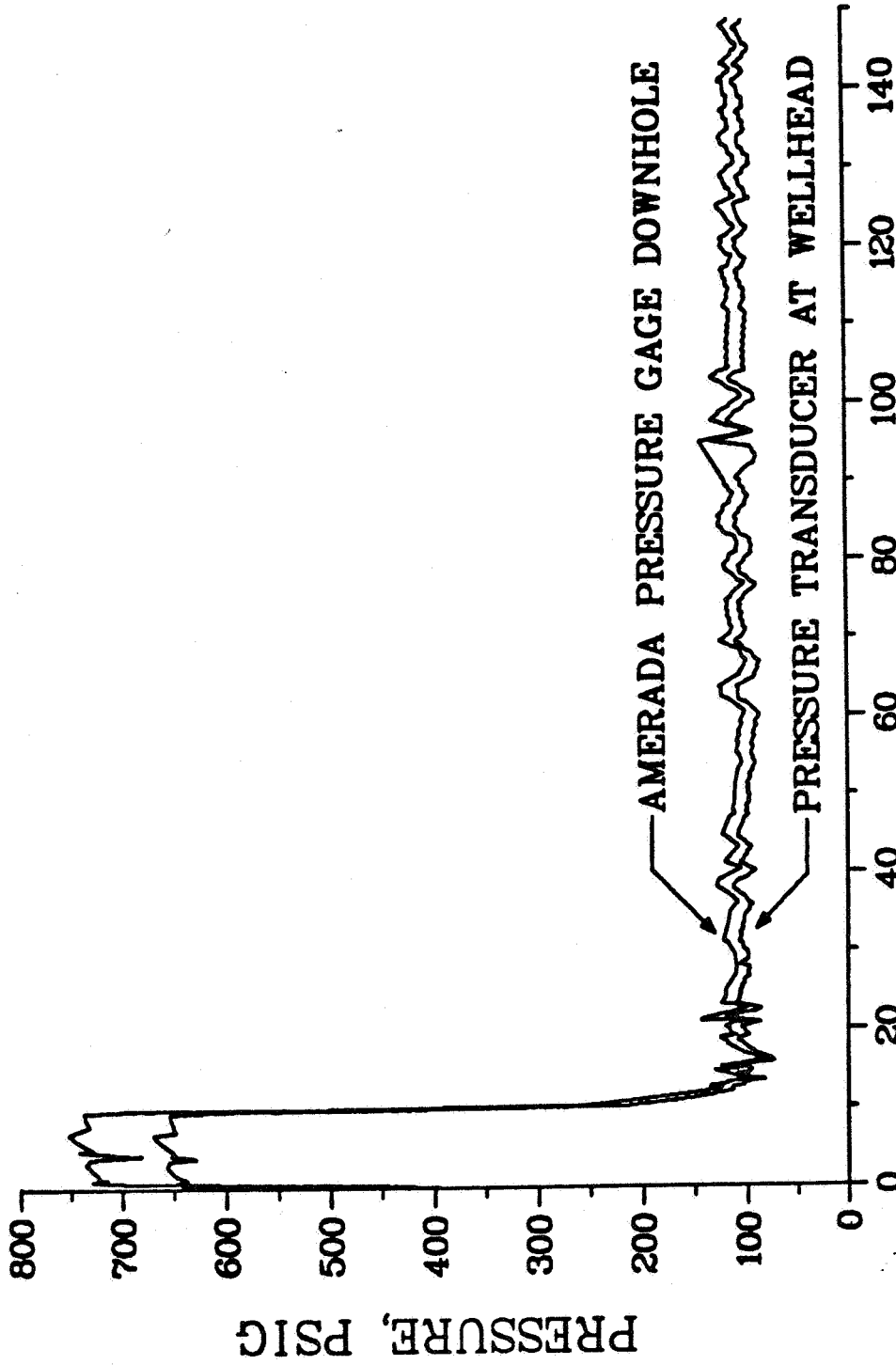


Figure 5. Effluent Tracer Concentrations at Wellheads



TIME ELAPSED IN TEST, HRS.

Figure 6. Comparison of Pressures Measured Downhole and at Wellhead in Well A

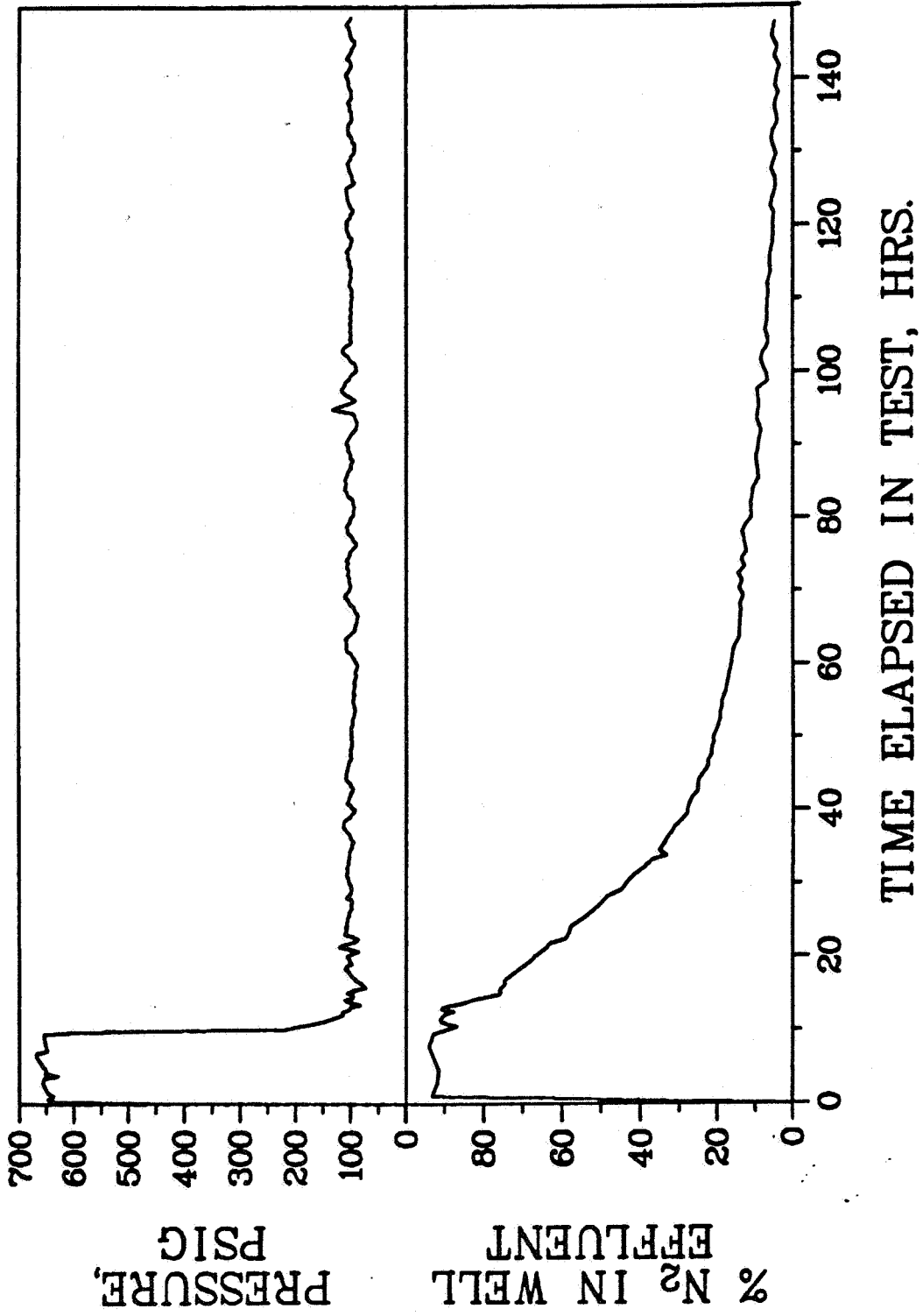
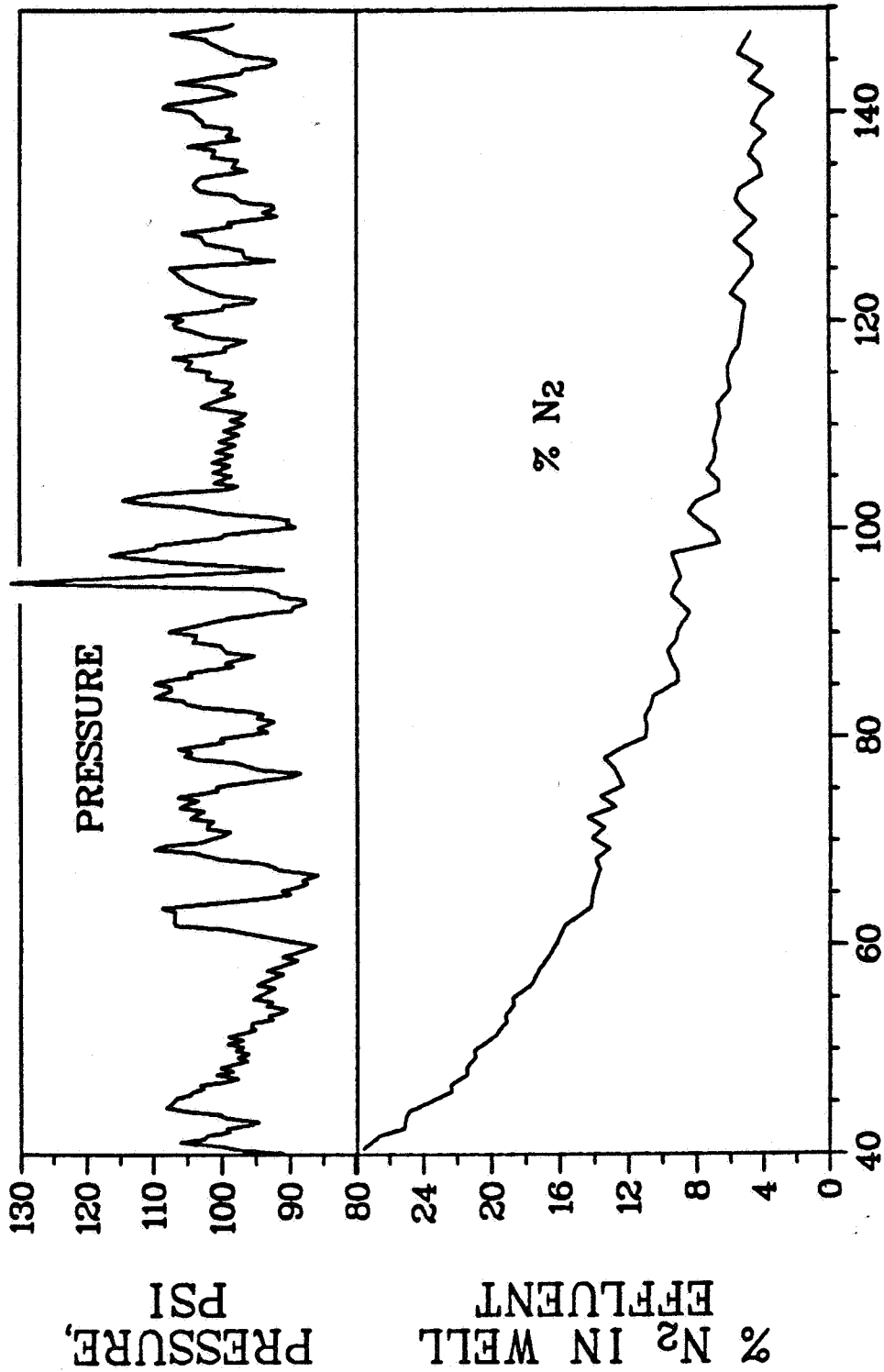


Figure 7. Wellhead Pressures and Tracer Concentrations in Well A



TIME ELAPSED IN TEST, HRS.

Figure 8. Wellhead Pressures and Tracer Concentrations in Well A during 100 psig Phase

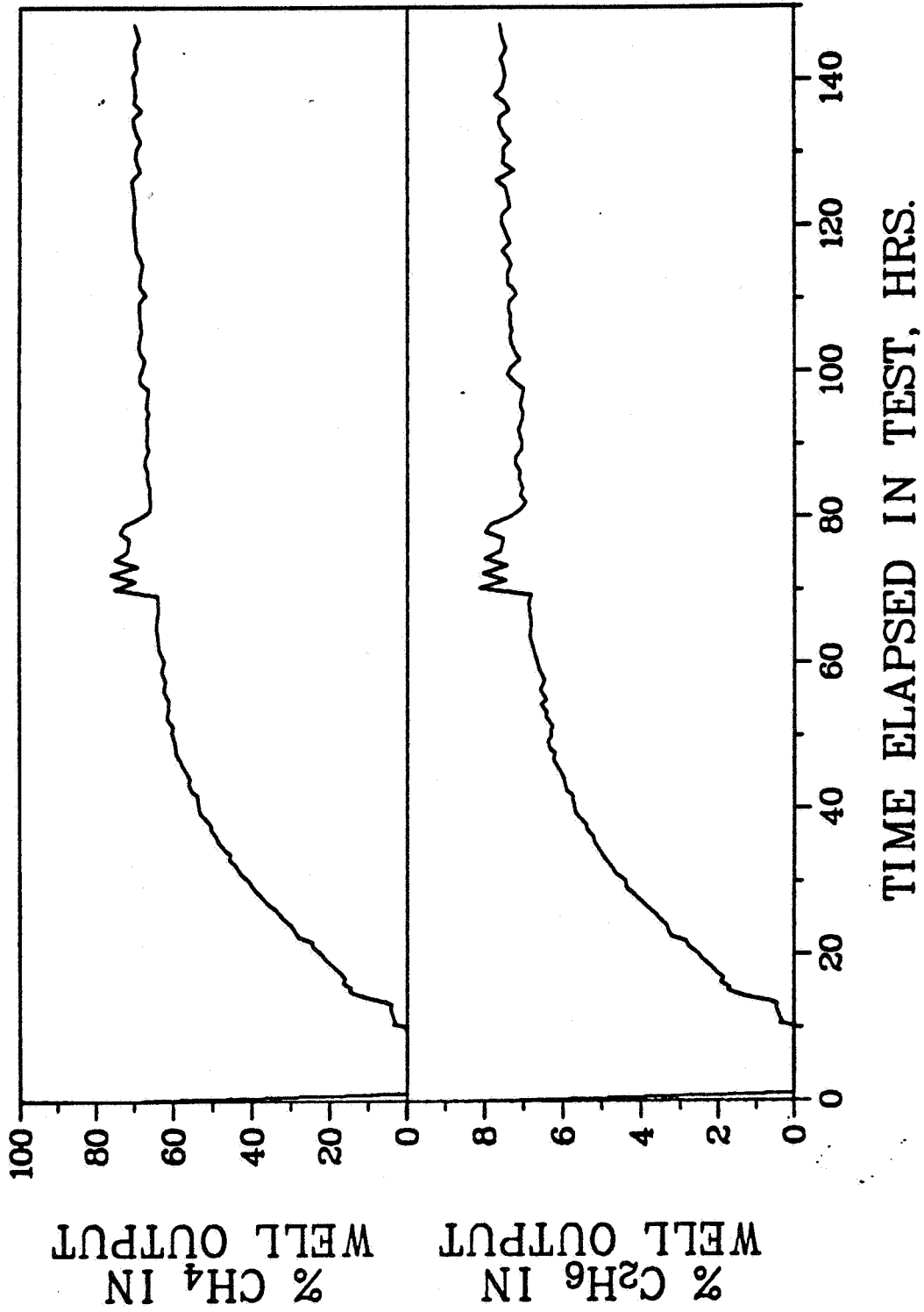


Figure 9. Concentrations of Methane and Ethane in Well A Effluent

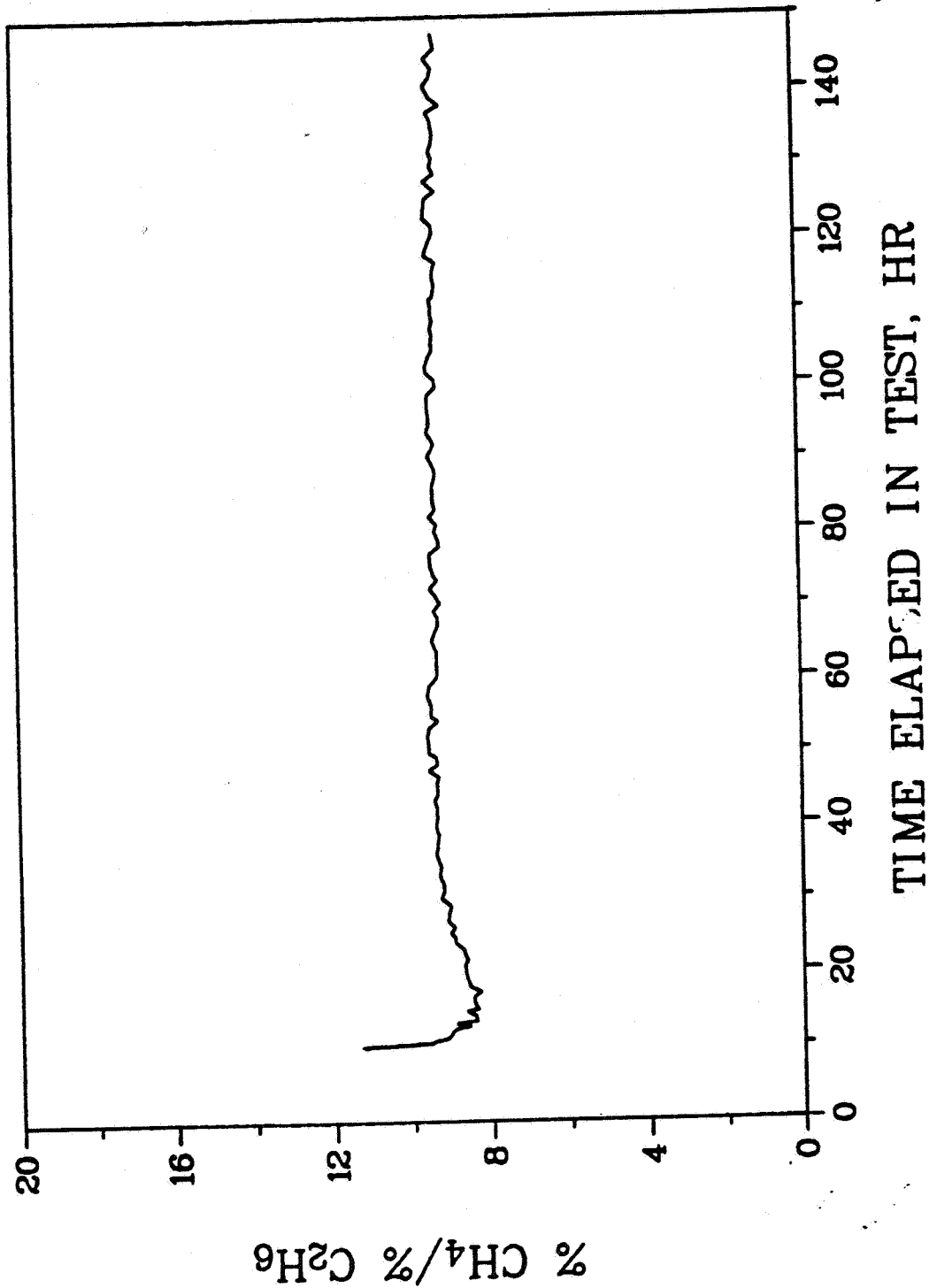


Figure 10. Methane/Ethane Ratio in Well A Effluent

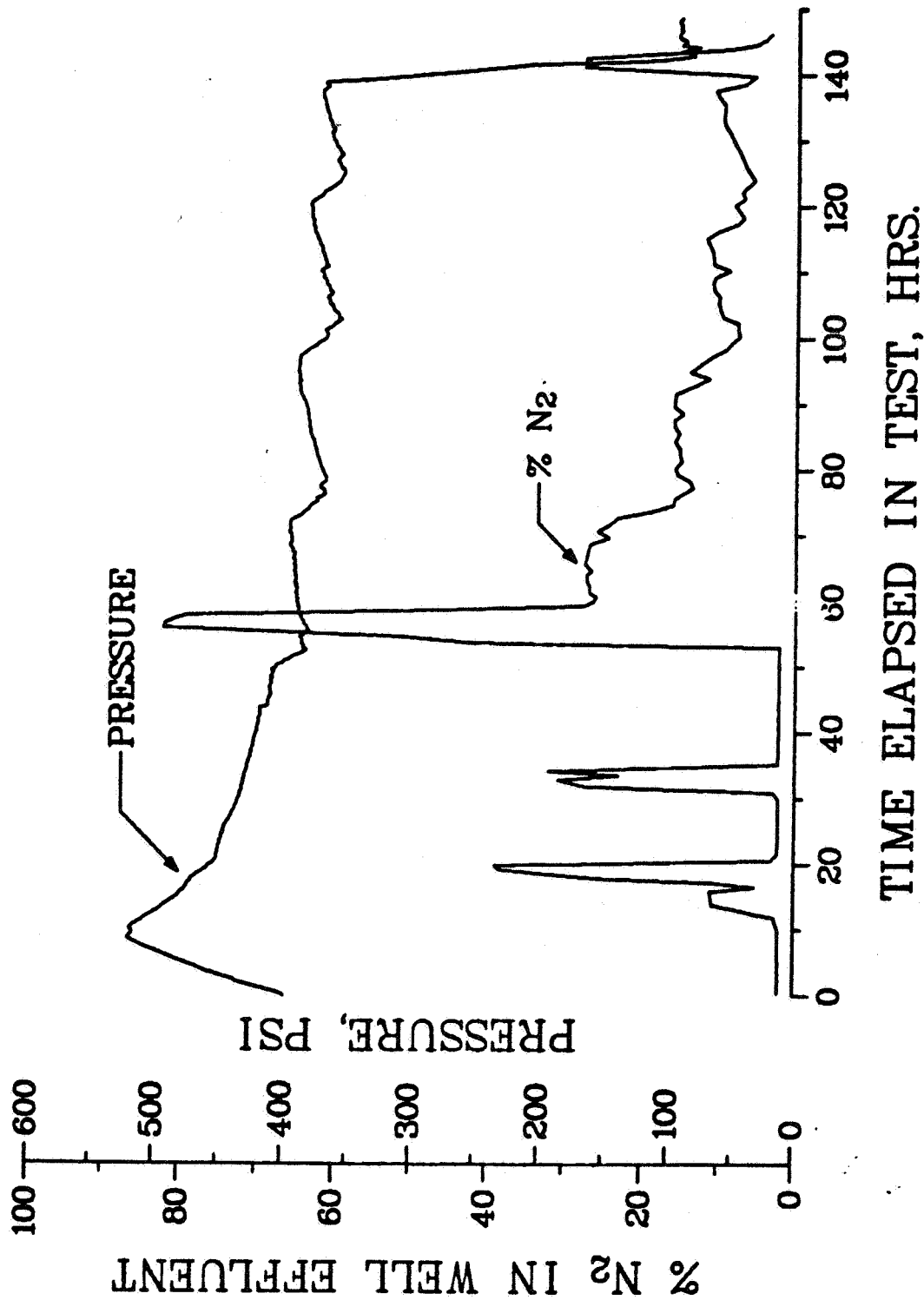


Figure 11. Wellhead Pressures and Tracer Concentrations in Well C Effluent

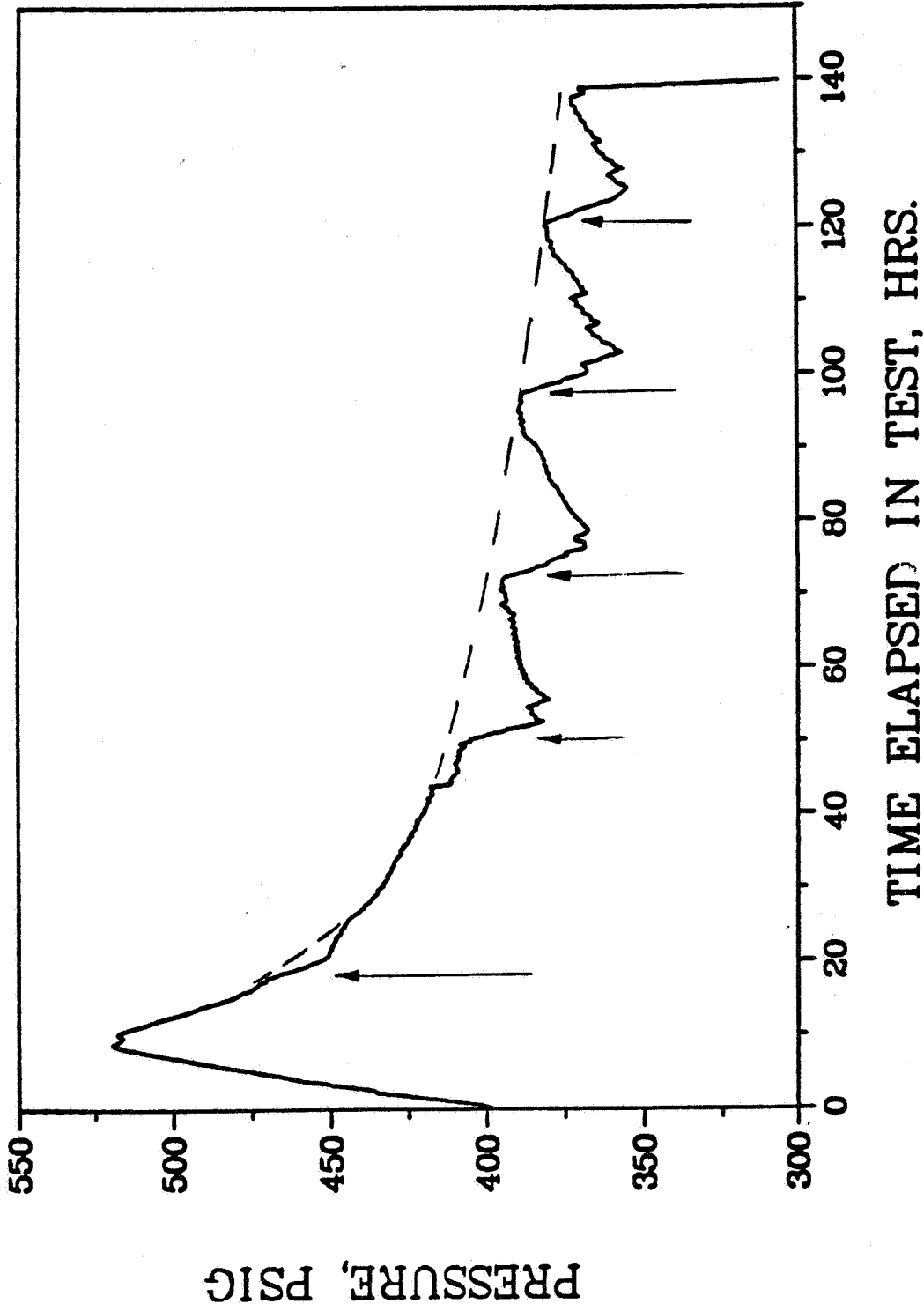


Figure 12. Occurrences of Major Leaks in Well C

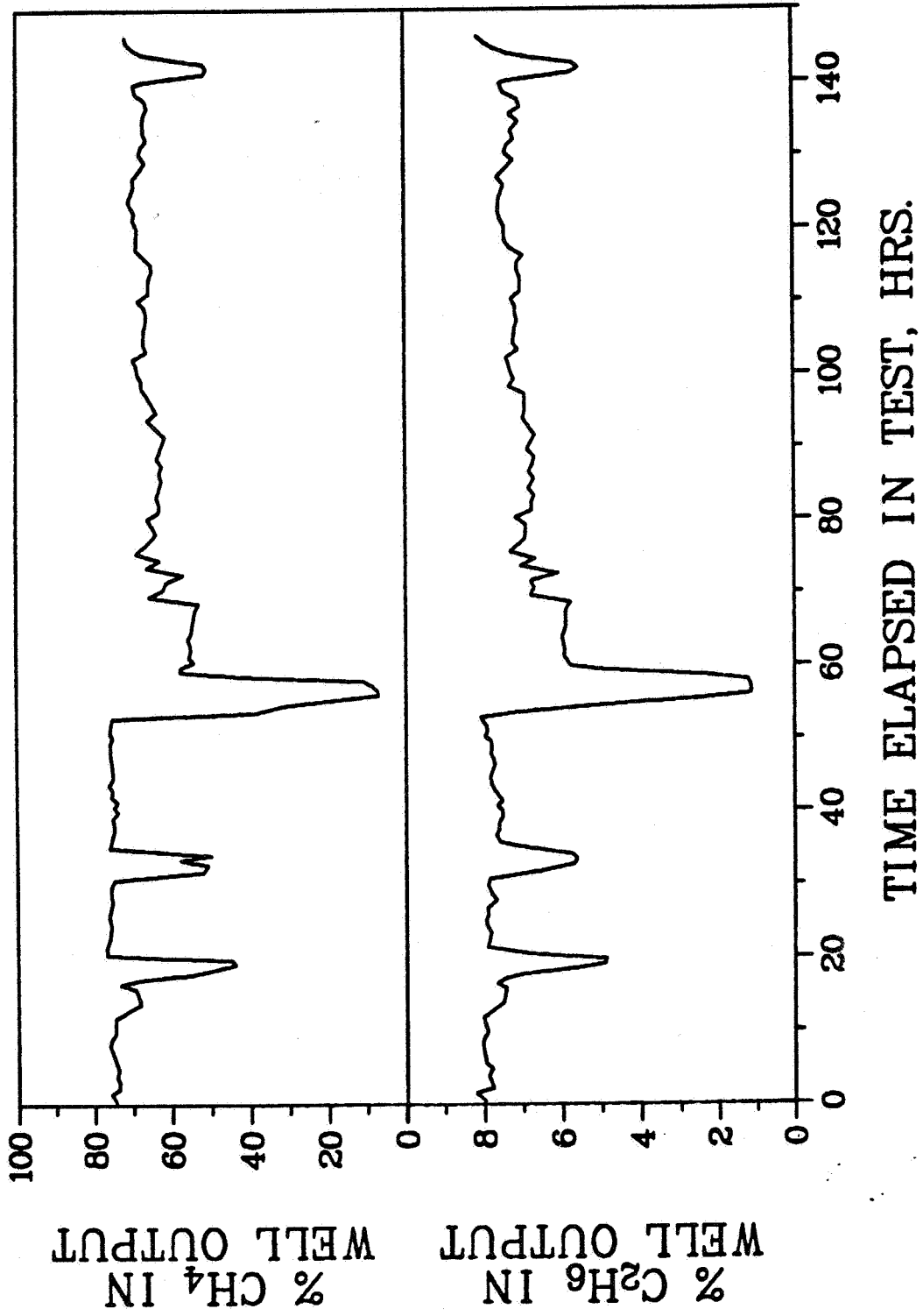


Figure 13. Concentrations of Methane and Ethane in Well C Effluent

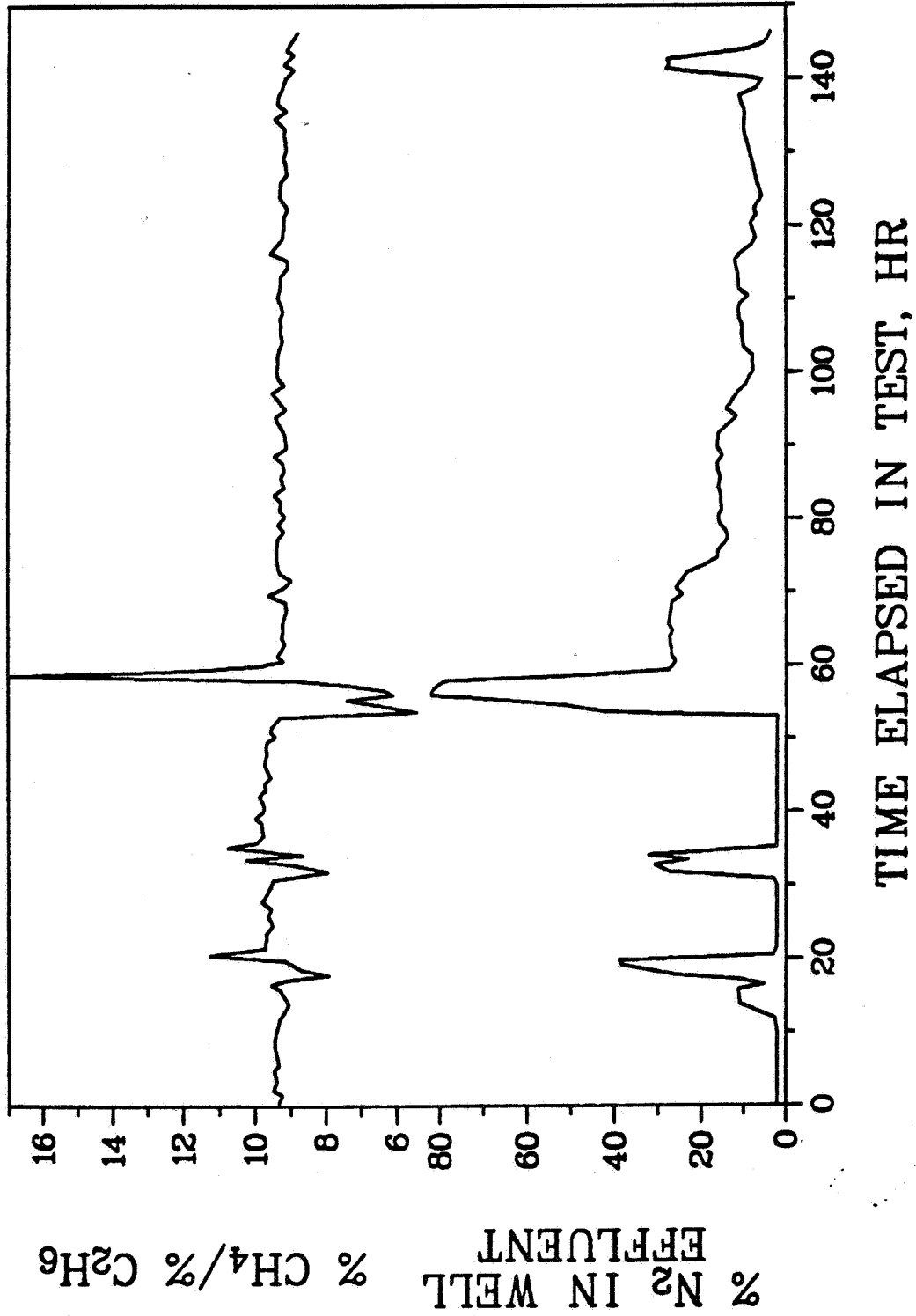


Figure 14. Methane/Ethane Ratio and Nitrogen Percentage in Well C Effluent

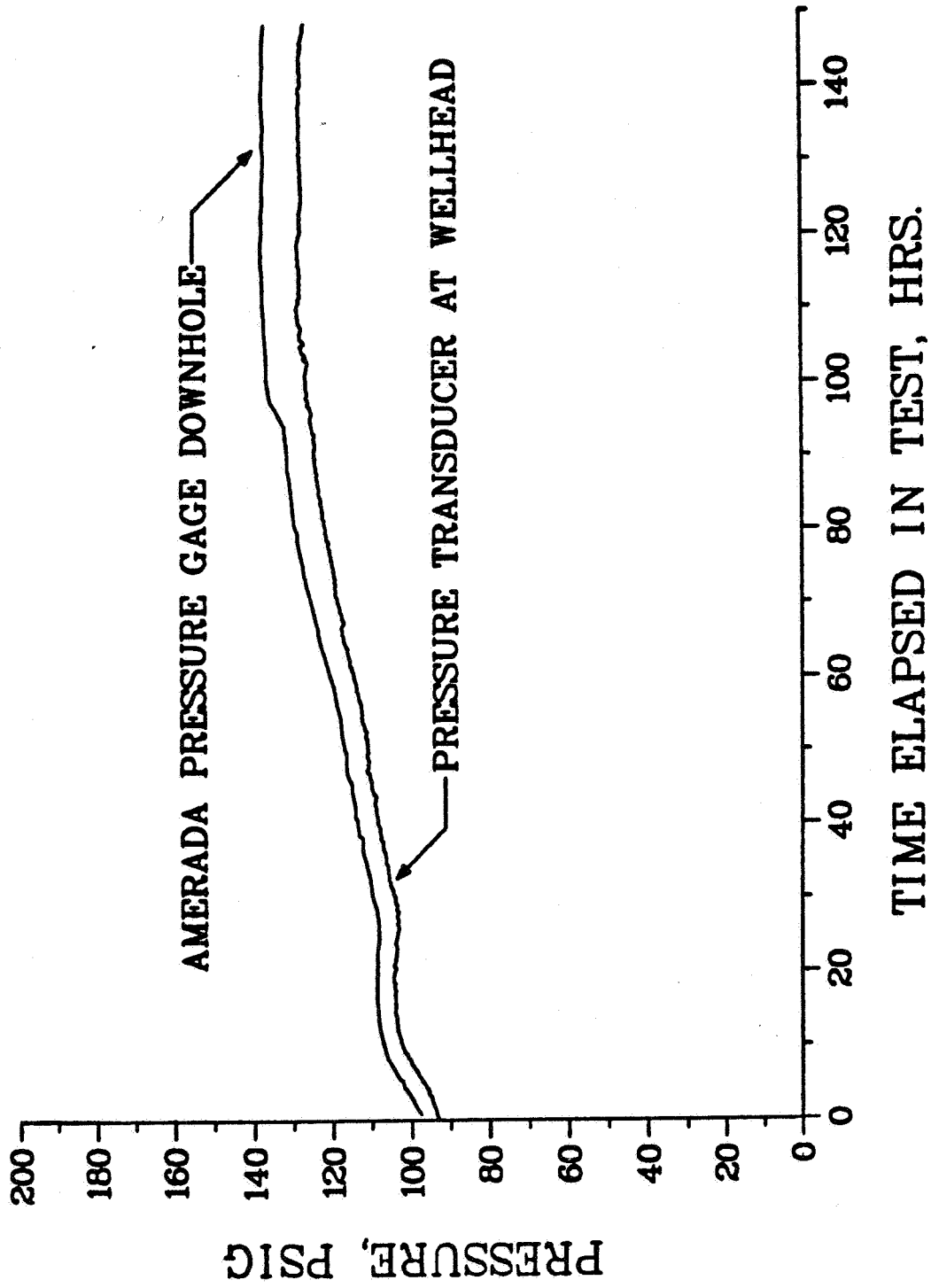


Figure 15. Comparison of Pressures Measured Downhole and at Wellhead in Well B

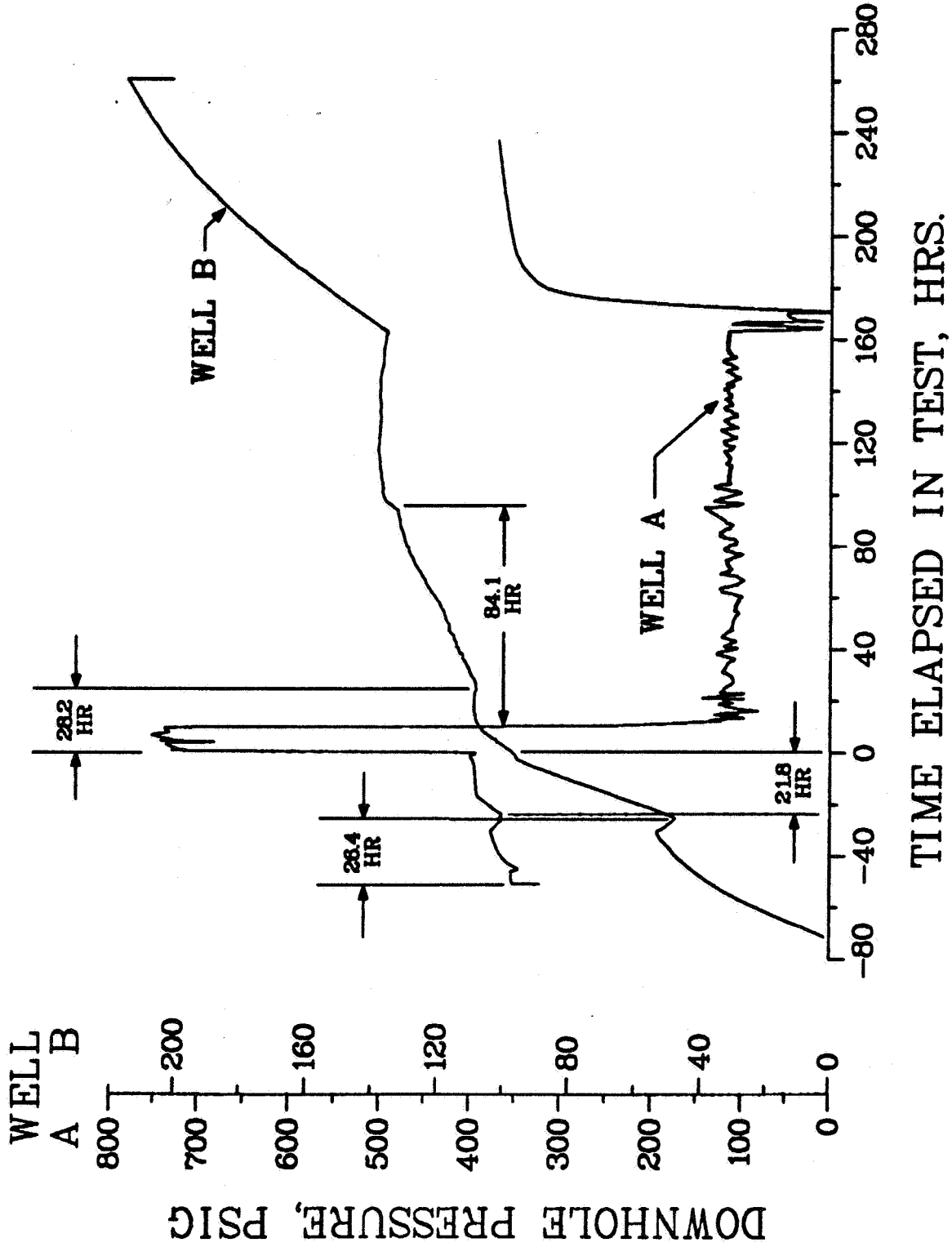
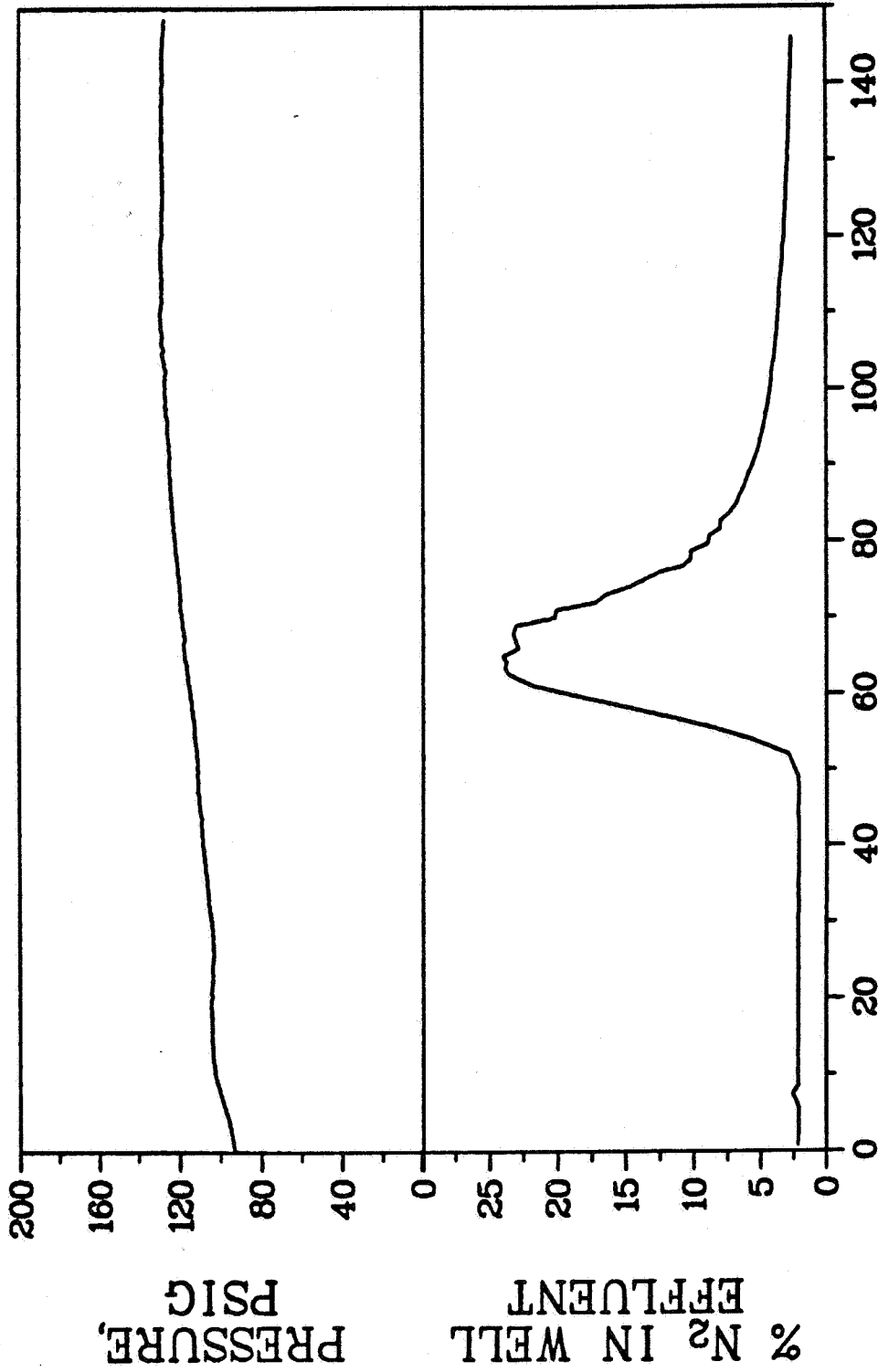
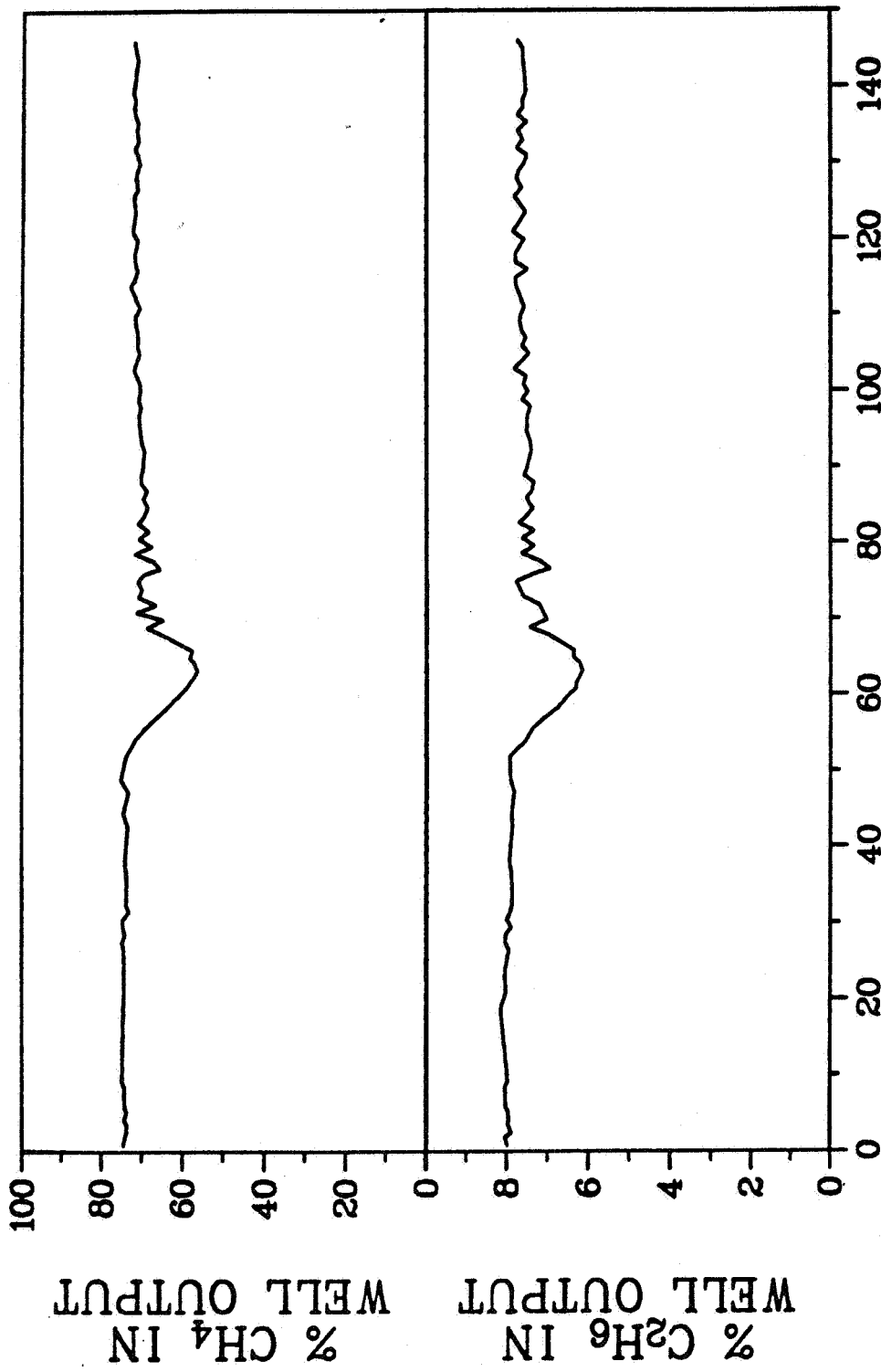


Figure 16. Use of A and B Downhole Pressures to Indicate Delay Times Between Events in Wells



TIME ELAPSED IN TEST, HRS.

Figure 17. Wellhead Pressures and Tracer Concentrations in Well B



TIME ELAPSED IN TEST, HRS.

Figure 18. Concentrations of Methane and Ethane in Well B Effluent

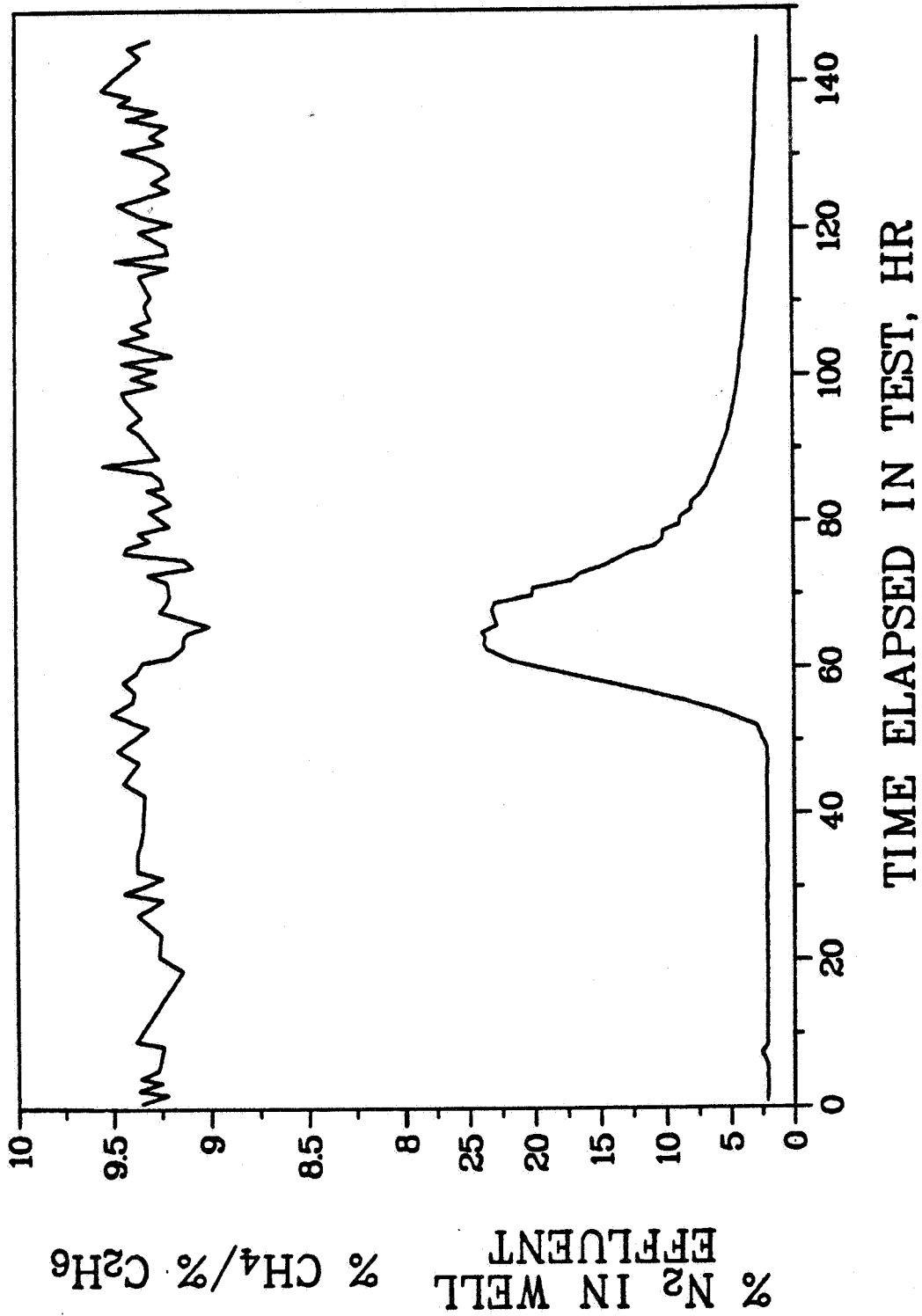


Figure 19. Methane/Ethane Ratio and Nitrogen Percentage in Well B Effluent

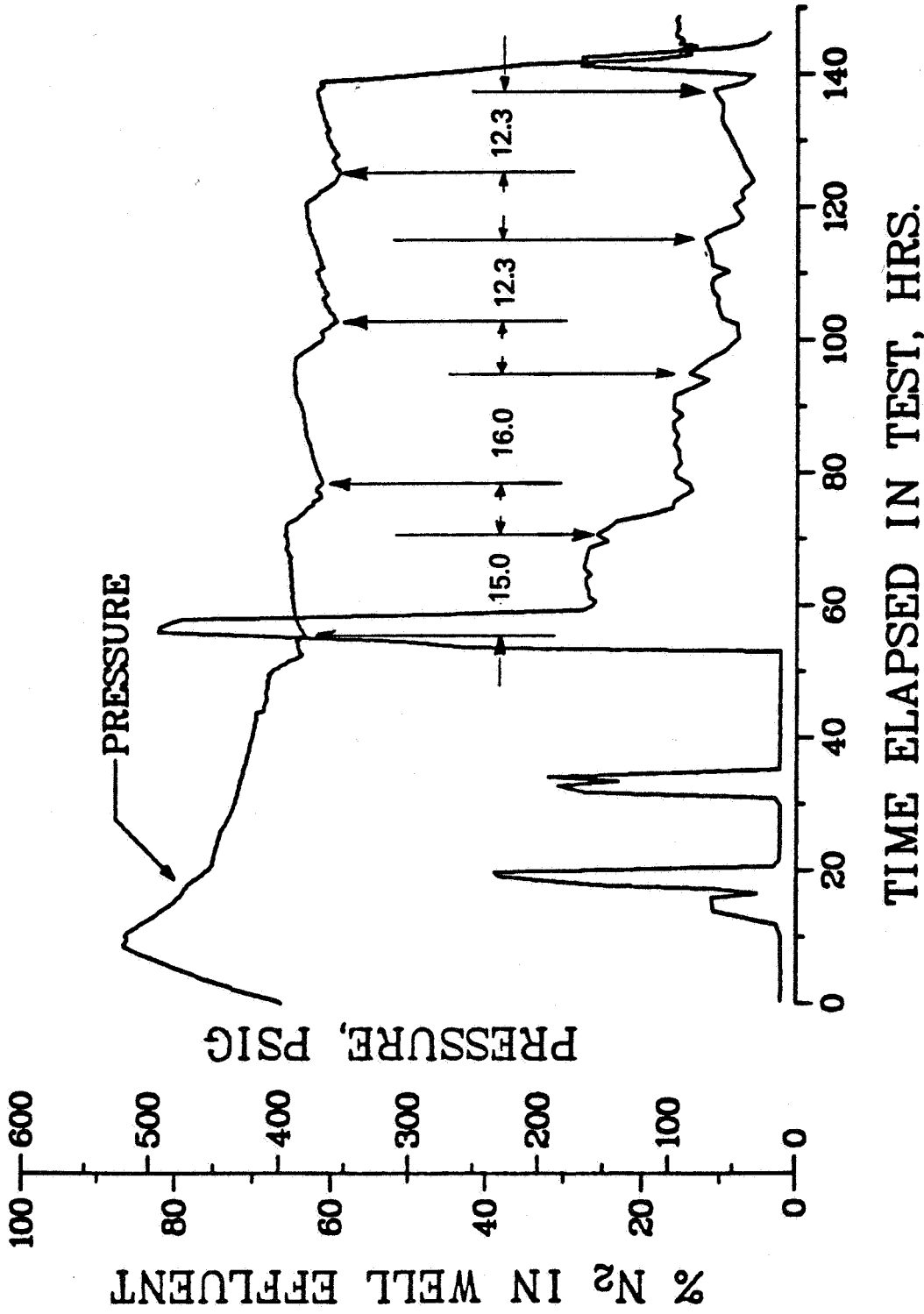


Figure 20. Time Lags between Stops of the Leak in Well C and Falls in Effluent Tracer Content

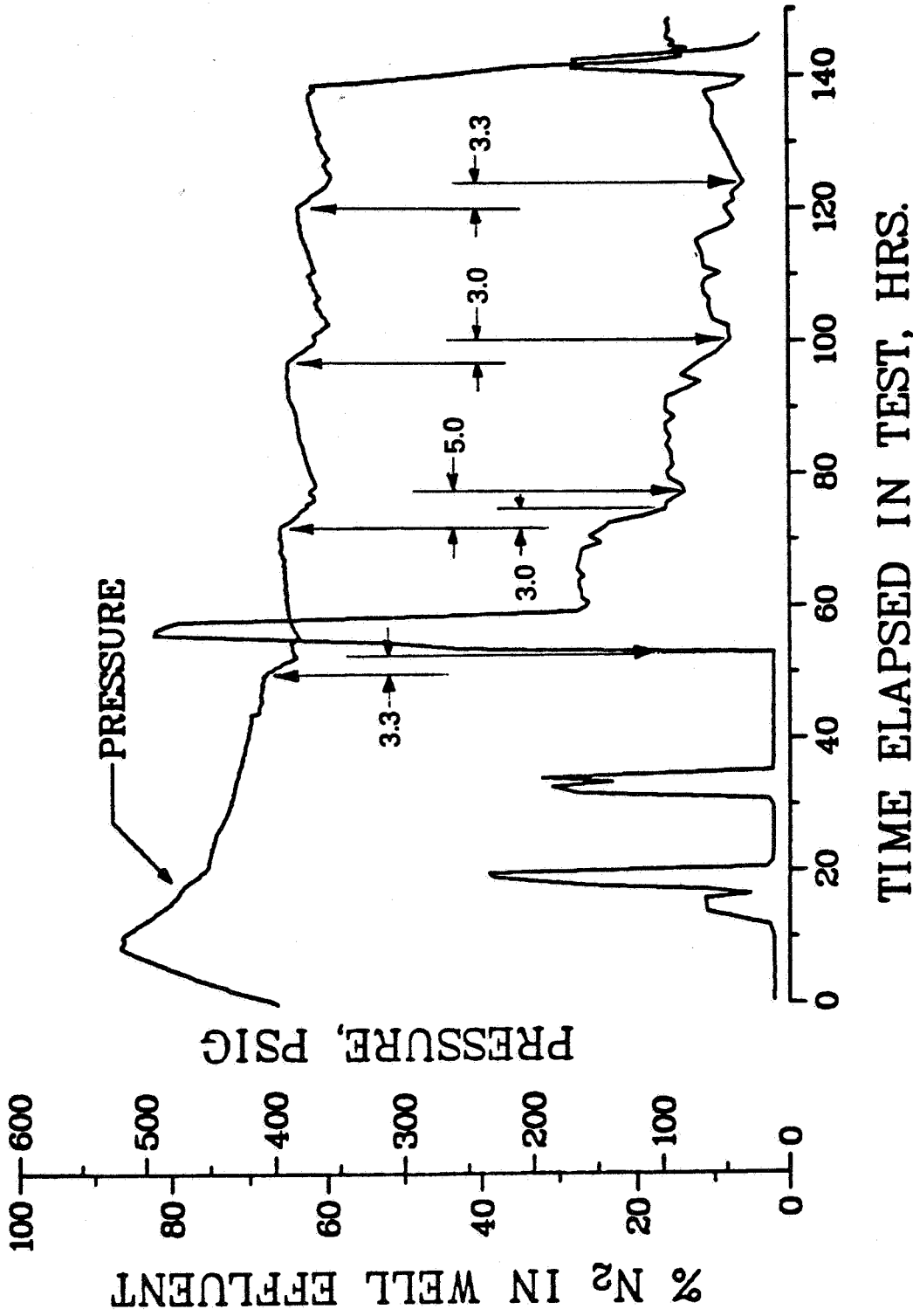


Figure 21. Time Lags between Starts of the Leak in Well C and Rises in Effluent Tracer Content

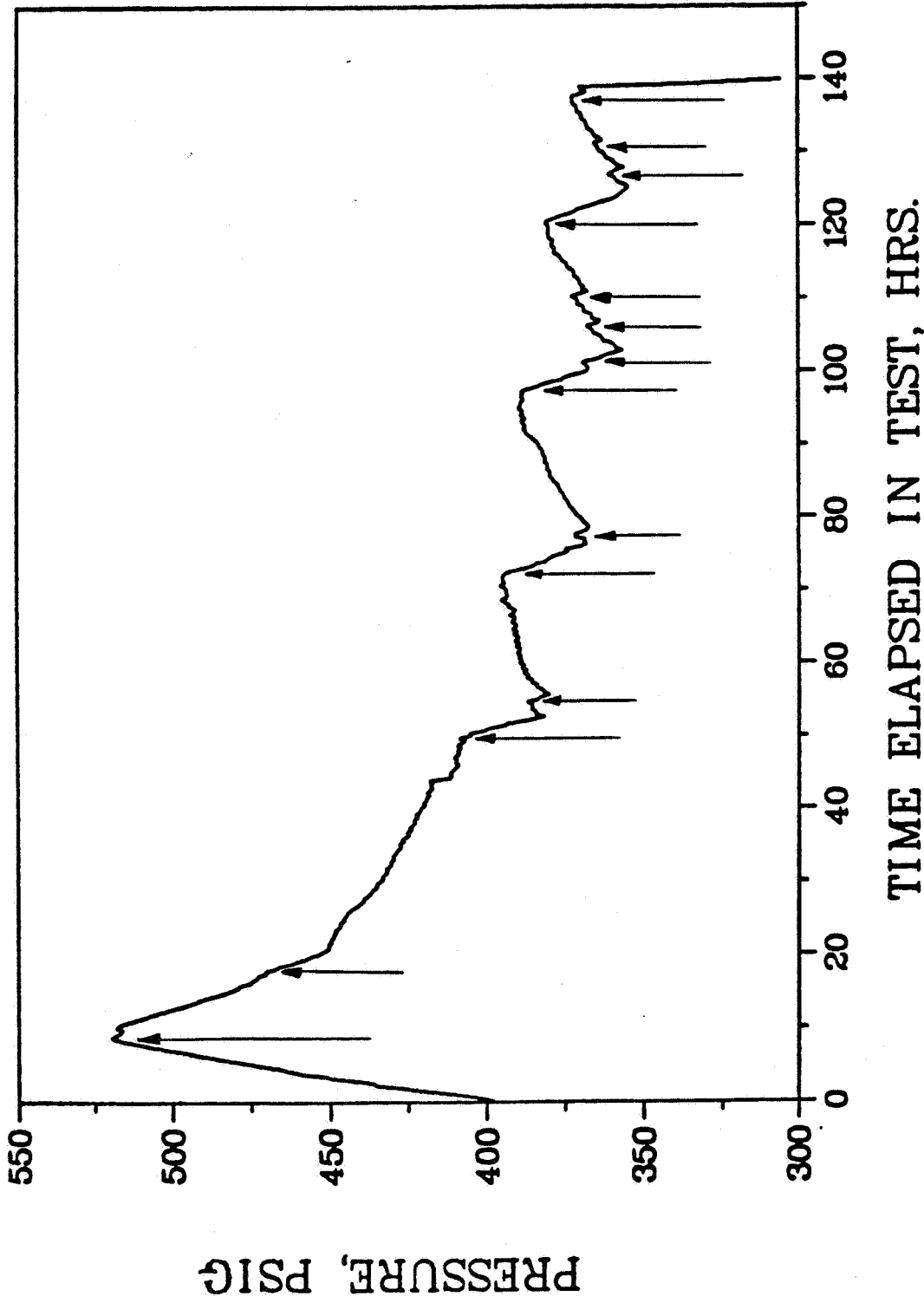


Figure 22. Occurrences of All Detectible Leaks in Well C

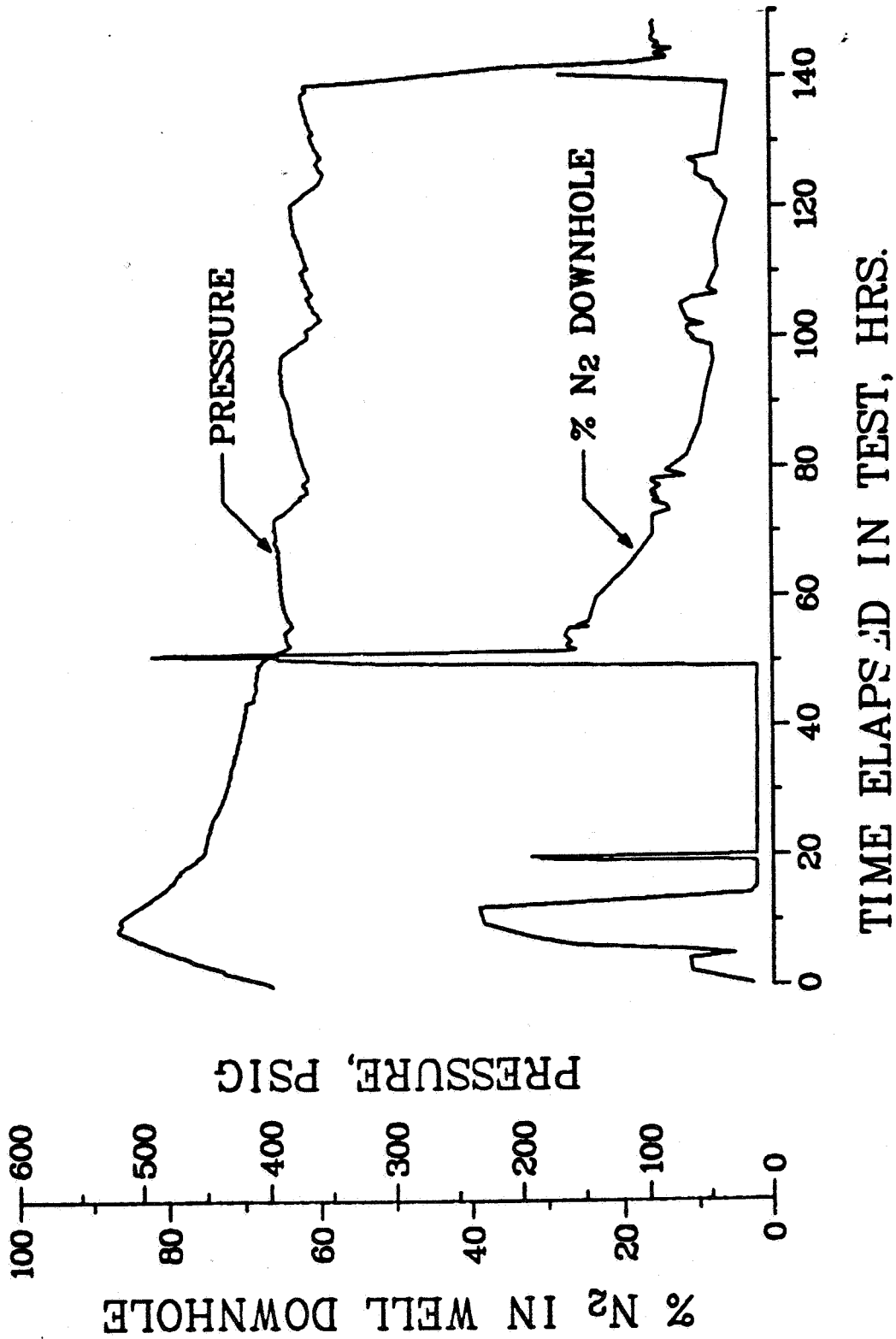
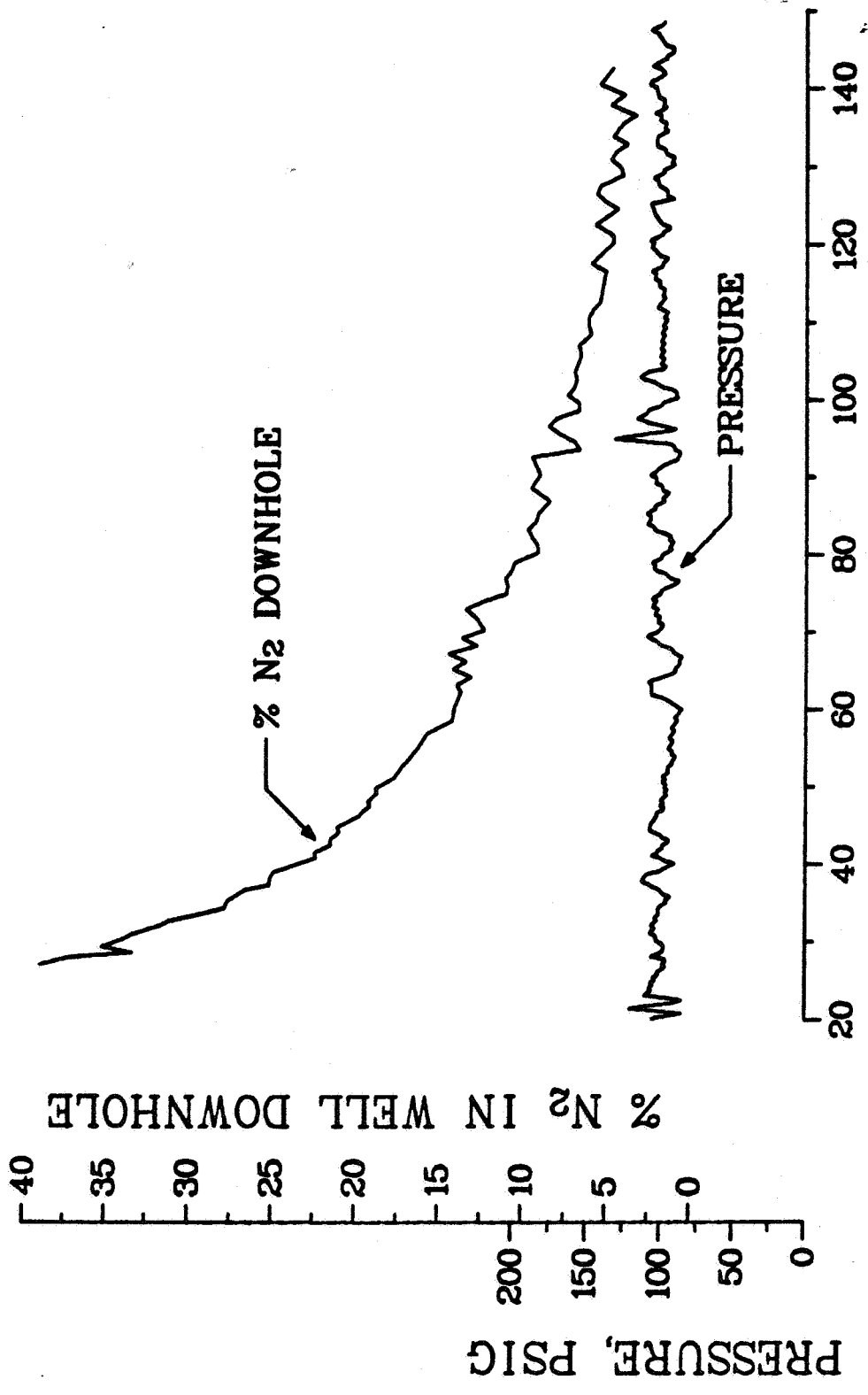


Figure 23. Wellhead Pressures and Downhole Tracer Concentrations in Well C



TIME ELAPSED IN TEST, HRS.

Figure 24. Wellhead Pressures and Downhole Tracer Concentrations in Well A during 100 psig Phase

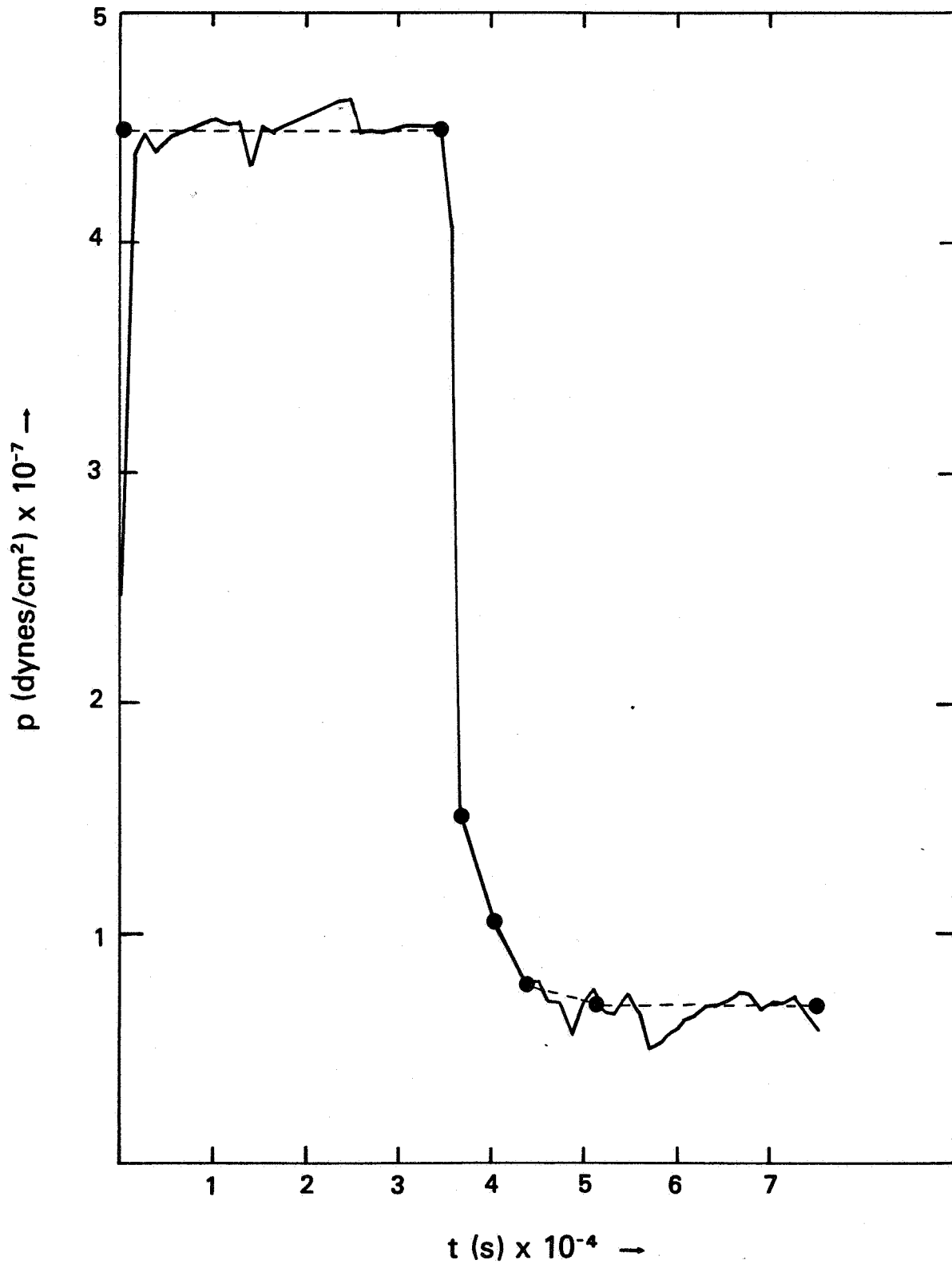


Figure 25. Measured Wellhead Pressures and Modeling Input for Well A

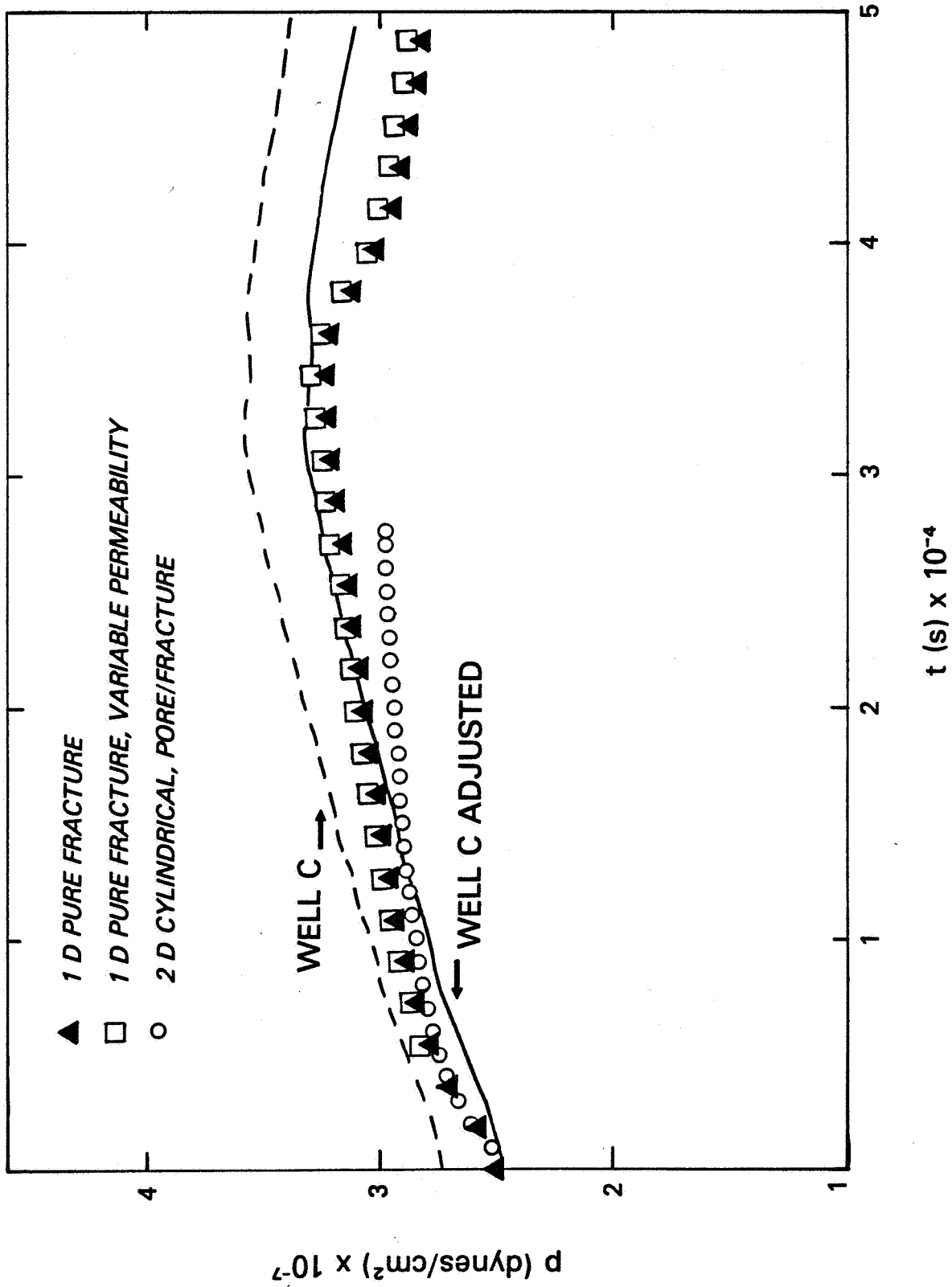


Figure 26. Preliminary Modeling Results

APPENDIX A  
MODELING AND EQUATION DERIVATION

We consider a single, penny-shaped fracture of half-height  $a$ , as illustrated in Fig. A1. We assume the flow in the fracture is steady, laminar, Poiseuille flow, for which we can write the velocity distribution

$$u(r,z) = u_0(r) \left(1 - \frac{z^2}{a^2}\right) , \quad (A1)$$

where  $u_0$  is the velocity in the center of the channel. The mean flow through the channel can be determined by considering the average velocity,  $\bar{u}(r)$ . We have

$$\begin{aligned} \bar{u}(r) &= \int_0^a u_0(r) \left(1 - \frac{z^2}{a^2}\right) dz / \int_0^a dz \\ &= \frac{2}{3} u_0(r) , \end{aligned} \quad (A2)$$

The stress,  $\sigma(r,z)$ , on each of the walls confining such a fluid is

$$\sigma(r,z) = - \mu \left( \frac{\partial u(r,z)}{\partial z} \right)_{z=a} , \quad (A3)$$

where  $\mu$  is the viscosity of the fluid. Combining Eqs. (A1) and (A3) we obtain

$$\sigma(r,a) = \frac{2\mu u_0(r)}{a} . \quad (A4)$$

To derive the dynamical balance for cylindrical flow in the fracture we refer to Fig. A2. We have

$$(p_1 - p_2)(r\delta\phi)(2a) = \frac{2\mu u_0(r)}{a} (2)(r\delta r\delta\phi) , \quad (A5)$$

which reduces to

$$\frac{p_1 - p_2}{\delta r} = \frac{2\mu u_0(r)}{a^2} . \quad (A6)$$

Expressed in terms of the velocity, Eq. (A2), describing the mean flow through the fracture, Eq. (A6) becomes

$$\frac{p_1 - p_2}{\delta r} = \frac{3\mu \bar{u}(r)}{a^2} . \quad (A7)$$

In the limit of vanishing  $\delta r$  we obtain

$$\frac{\partial p}{\partial r} = \frac{3\mu \bar{u}(r)}{a^2} . \quad (A8)$$

The compressibility of the gas is included by writing the continuity equation. In one-dimensional cylindrical coordinates the equation is

The fracture porosity is defined as the volume of the fractures divided by the total volume of the system,

$$\theta_f = \frac{2a}{w} \quad . \quad (A12)$$

The permeability is a measure of the resistance a medium offers to the flow of a fluid through it. The permeability is defined in terms of the discharge velocity by the equation,

$$\frac{p_1 - p_2}{L} = \frac{\mu u_d}{k_f} \quad . \quad (A13)$$

From conservation, we have

$$\theta_f \bar{u} = u_d \quad . \quad (A14)$$

Hence,

$$\frac{p_1 - p_2}{L} = \frac{\mu \theta_f \bar{u}}{k_f} \quad (A15)$$

In the limit of vanishing L, Eq. (A15) becomes

$$-\frac{\partial p}{\partial r} = \frac{\mu \theta_f \bar{u}}{k_f} \quad (A16)$$

Combining Eqs. (A8), (A12), and (A16) we obtain an expression that

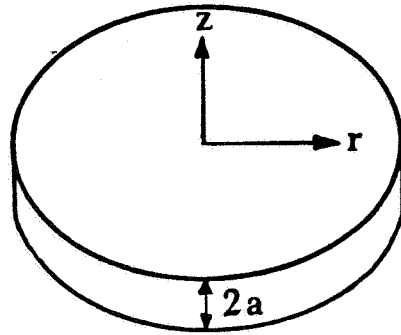


Figure A1. Penny-Shaped Fracture

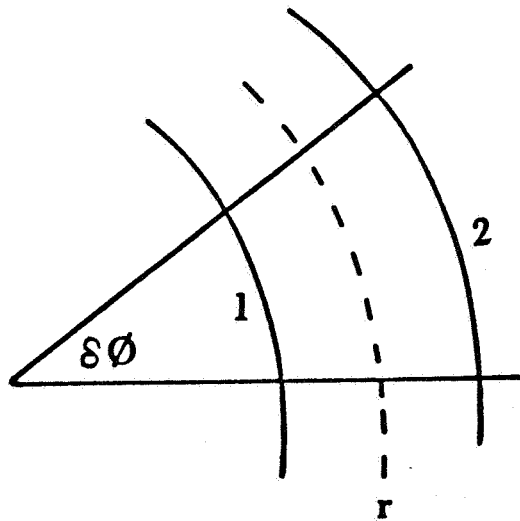


Figure A2. Calculational Cell in Cylindrical Geometry

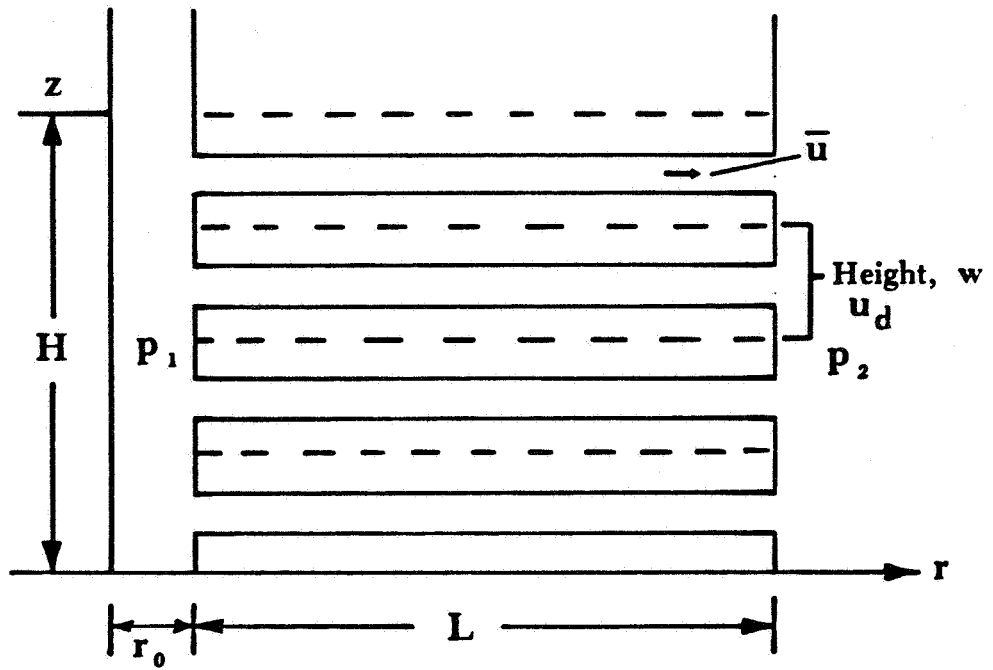


Figure A3. Cross Sectional View of the Cylindrical Model

APPENDIX B  
PRE-TEST SIMULATIONS

The pre-test simulations used the sequential injection of nitrogen and carbon dioxide. Perhaps the most important conclusion from these simulations resulted from the predicted concentration-time histories for the base case and for a variation in which the permeability of the rock matrix system was increased by a factor of a hundred. For Well A at a constant back-production flow rate, the concentration-time histories of methane, nitrogen, and carbon dioxide from the higher-matrix-permeability situation were indistinguishable from the histories of the base case presented in Fig. B3. For the three gases coming from Well C, no essential qualitative differences were seen in the concentration-time histories. There were some quantitative differences, but for any real system there would be insufficient knowledge to distinguish between the two situations. This meant that injecting nitrogen and carbon dioxide sequentially might well not distinguish between the fracture-system flow or flow from the matrix as being the primary source of methane in the system. As a result of this conclusion, alternative experimental procedures were considered for achieving the desired goal.

Other important conclusions were reached from the simulations. The results showed that the most sensitive parameter was the assumed fracture spacing. It was also concluded that the relatively high matrix porosity used in the study delayed the arrival of the injected gases at Wells B and C significantly, softening the effect of the fractures. If the matrix porosity had been less, the sensitivity of the results to the fracture modeling would have been even greater. This indicates that matching between simulated and experimental results will give a realistic and rather precise model of a fracture system.

Thus the simulation study reported here made two important contributions to the investigation. It caused us to seek another (and in the event, simpler) experimental strategy, and it forecast that we would be able to

TABLE BI  
Reference Calculation

Bulk Density, $\rho$ :	2.2 g/cm <sup>3</sup>
Fracture Spacing	
x-direction, $L_x$ :	5.0 m
y-direction, $L_y$ :	5.0 m
Porosity	
matrix, $\theta_m$ :	5.0%
fracture, $\theta_f$ :	1.0%
Permeability	
matrix, $k_m$ :	1.0 md
fracture, $k_f$ :	25.0 $\mu$ d

dimensional flow in a plane of unit thickness corresponding to a horizontal bed.

Table BII lists the four variations from the base case. Each calculation was identical to the base calculation except for the single detail listed. In the first variation we increased the matrix permeability by a factor of 100. In the second we assigned a uniform but anisotropic fracture distribution; we increased the fracture separation in the x-direction to 20 m. In the third variation we introduced the effects of an explosive gas fracture, extending from the main production well, Well C, to the halfway point between Wells A and C. The permeability of this single fracture was 10 md, while the permeability of all other fractures remained 25  $\mu$ d. The fourth variation simulated springing of the main production well, in which the permeability of the pore matrix was equated to the fracture permeability, 25  $\mu$ d, within a region of shale extending 2 m in all directions from C.

days, respectively. At a time of 4 days the tracer injection, has just stopped, and back-production has begun at Well A.

The detailed structure of the pressure contours shows very well the local delay in equilibrium between each individual shale block and the surrounding fractures. The fracture network is especially evident in the outer regions, where the pressure gradient between the open channels and the shale blocks was still confined to the periphery of each block. Contours within the shale blocks were square at the beginning of pressure equilibration and evolved toward smaller and smaller circles as equilibration proceeded. The highly complicated contour structure near the injection well indicates that the pressures in the channels and blocks had not equilibrated in the central region at that time. Wells B and C are visible as distortions of the pressure field from bilateral symmetry. The outermost pressure contour in Fig. B1A is 40 bars; the innermost, 48 bars.

The CH<sub>4</sub> concentration, which indicates the ratio of the number of grams of the species to the total gas mass in a given location, is shown in Fig. B1B. We assumed an initial CH<sub>4</sub> concentration of 1.0. As the tracer gases were injected, the CH<sub>4</sub> was displaced. The outermost contour in Fig. B1B is 0.9. As we proceeded inward toward the injection well, the CH<sub>4</sub> concentration decreased. The contour levels correspond to those defined in Table IV. Figures B1C and B1D show the concentration contours for N<sub>2</sub> and CO<sub>2</sub>, respectively. The outermost contour is 10<sup>-7</sup>; the innermost, 0.9. The global pattern of each of these concentration maps resembles a square with slight elongation in the direction of the main production well. The pattern is not circular because of the preferential channeling built into this block/fracture network model.

Figure B2 shows the same variables at 11 days, 7 days after back-production commenced at the injection well. The pressure field had equilibrated in the outer regions. Gradients were evident in the vicinity of all three wells. The contours nearest each well represent the 40 bar level. The global patterns of the concentration contours still resembled rotated

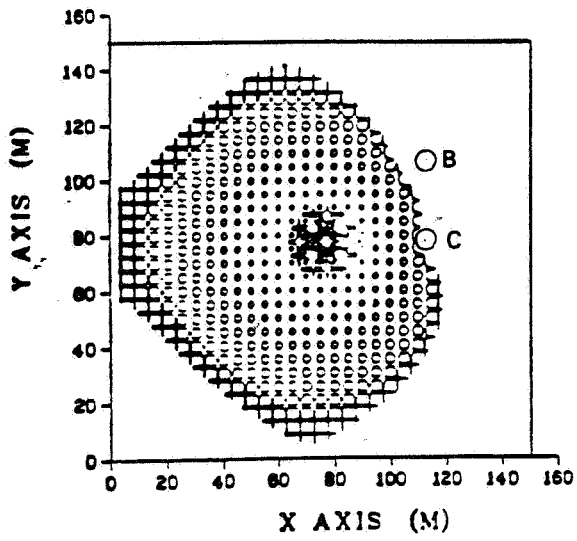
Figures B5-B8 compare the four calculational variations from the base case. Figure B6 presents the pressure contours at 4 days. The almost circular global pattern in Fig. B5A resulted because of the increased pore permeability. This situation allowed the pressure to equilibrate more rapidly in each pore block; hence a much slower propagation of the pressure pulse resulted allowing more time for expansion of the front in the diagonal directions. A slight flattening of the front indicates the presence of Wells B and C. This pattern is very different from the pressure contours for the base case at this time, Fig. B1A. Figure B5B accentuates the anisotropy of the channeling effect of the fracture network, which directed the flow preferentially in the x-direction. Figure B5C shows that the effect of the assumed large crack in the explosive fracture case on the pressure field to be minimal; i.e., Figs. B5C and B1A are very similar. The crack does however result in a large alteration of the tracer concentration at Well C. Springing of Well C affected the pressure field even less than the gas fracture, as shown in Fig. B5D.

Figures B6, B7 and B8 show the concentrations of  $\text{CH}_4$ ,  $\text{N}_2$  and  $\text{CO}_2$ , respectively, at Well C for the four variations from the base case. Figures B6A and B6D are similar to the base case. Very little  $\text{CH}_4$  displacement was observed at the main production well. Figures B7A and B8A show that the  $\text{N}_2$  and  $\text{CO}_2$  concentrations at Well C for the calculation in which we increased block permeability are reduced by a factor of about 2/3 from the base case. Figures B7D and B8D show that this factor is approximately 1/2 for the well springing case.

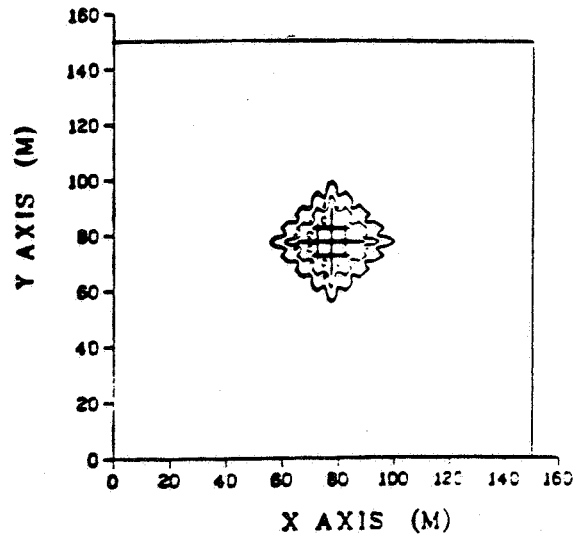
The calculation in which we varied the channeling properties of the medium by increasing the fracture spacing in the x-direction and the explosive fracture calculation do show extensive differences in tracer concentration at Well C, and correspondingly in  $\text{CH}_4$  concentration there. The  $\text{CH}_4$  displacement in the case of increased crack spacing, Fig. B6B, was less localized than the displacement that resulted in the explosive fracture case. That is, the open channel in the latter case more effectively swept the  $\text{CH}_4$  away from the immediate vicinity of Well C. The  $\text{CH}_4$  dip was hence deeper and

less, the sensitivity of the results to the fracture modeling would have been even greater. Even so, the most sensitive parameter in the model was the assumed fracture spacing. Thus comparing modeling results and experimental data will lead to a realistic and precise model of a fracture system.

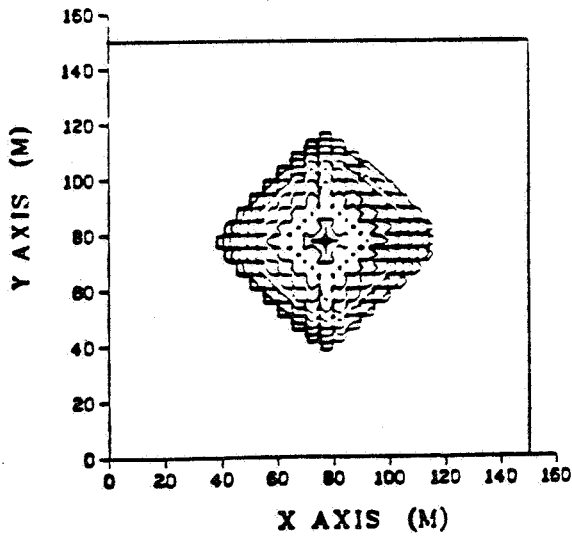
In conclusion, it is seen that the pre-test simulations led to changing the experimental strategy of the tracer test. In addition, the modeling has shown that the underground system can be characterized well by matching experimental results with post-test simulations.



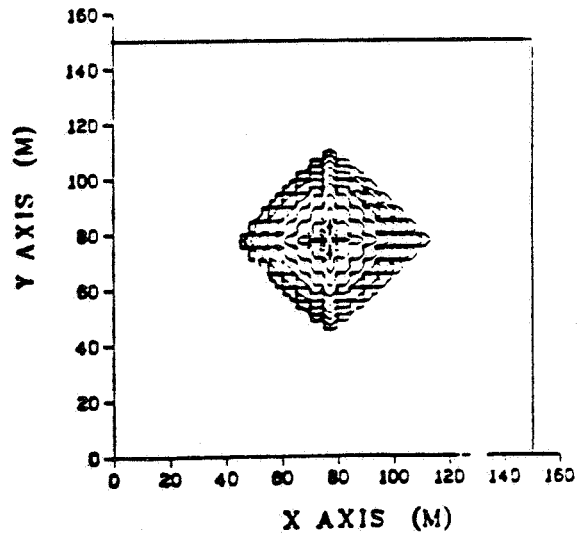
A. Pressure



B. CH<sub>4</sub> Concentration

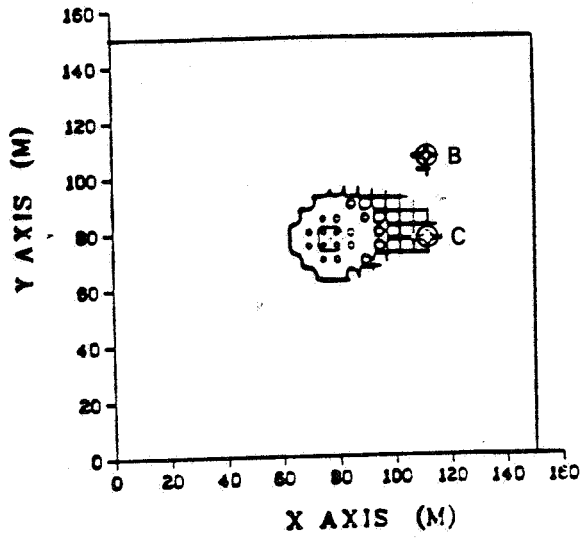


C. N<sub>2</sub> Concentration

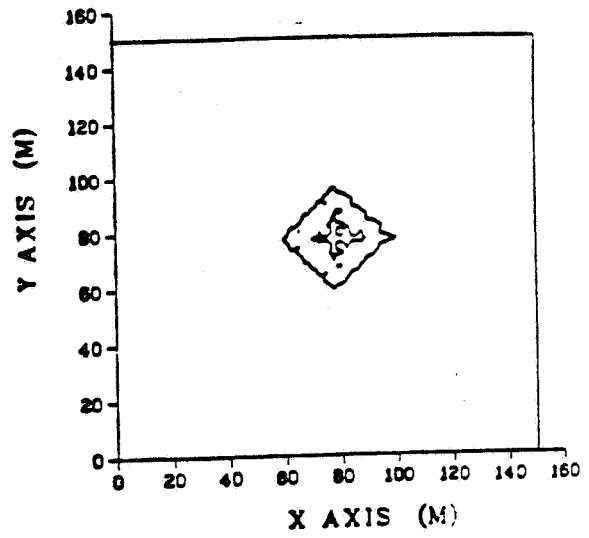


D. CO<sub>2</sub> Concentration

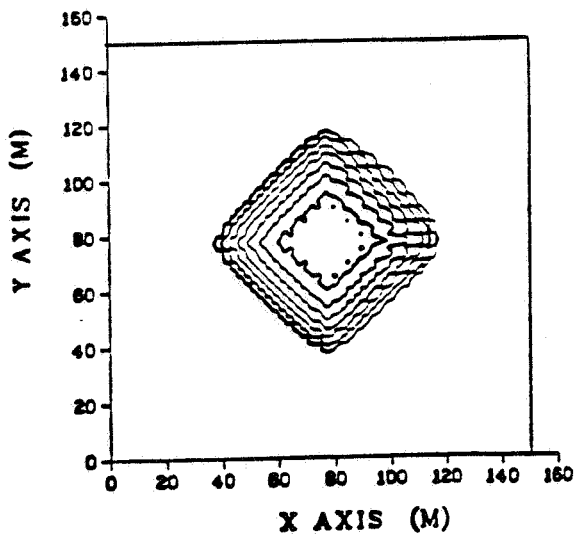
Figure B1. Pre-Test Simulations; Base Case at 4 Days



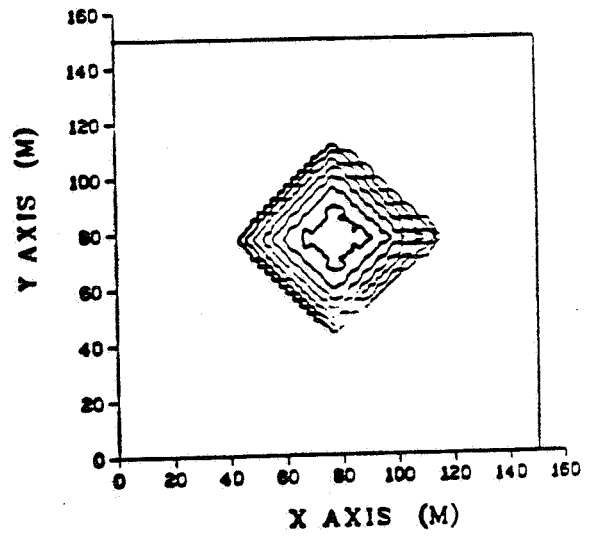
A. Pressure



B. CH<sub>4</sub> Concentration



C. N<sub>2</sub> Concentration



D. CO<sub>2</sub> Concentration

Figure B2. Pre-Test Simulations; Base Case at 11 Days

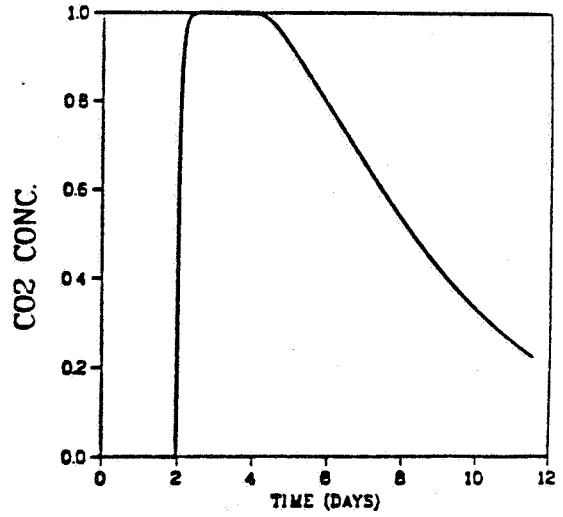
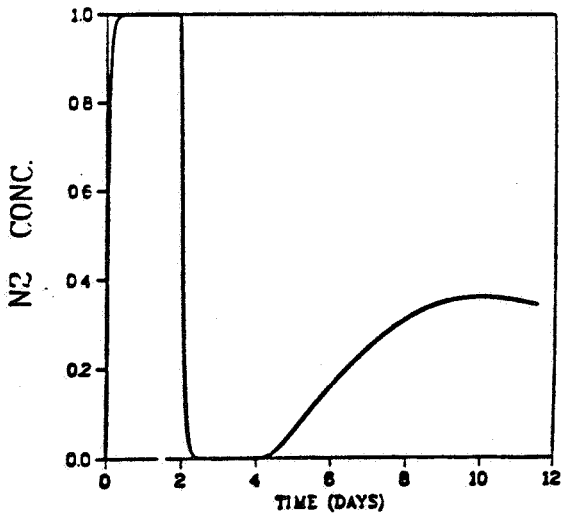
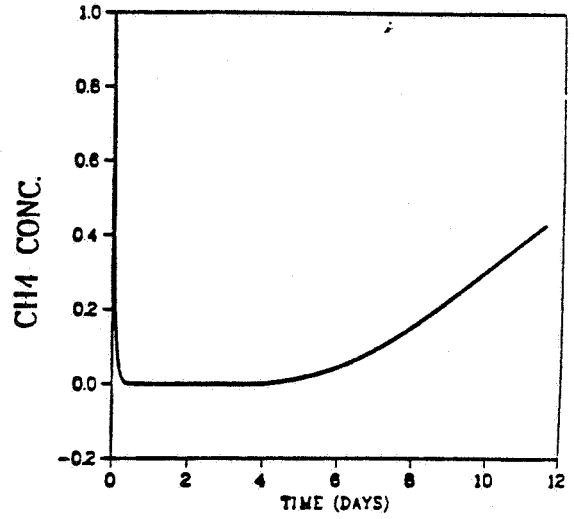
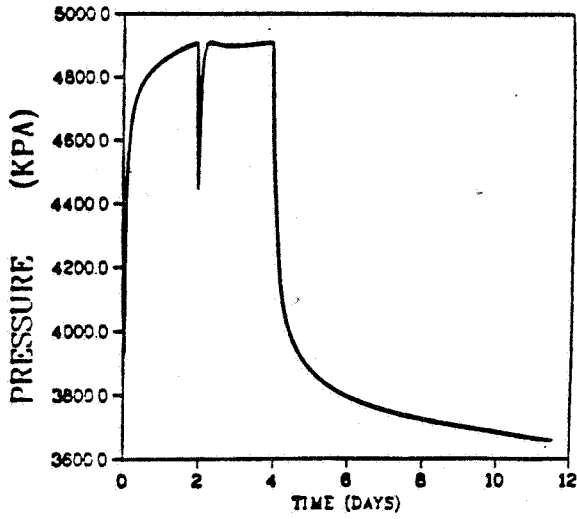


Figure B3. Pre-Test Simulations; Well A Pressure and Concentration-Time Histories for the Base Case

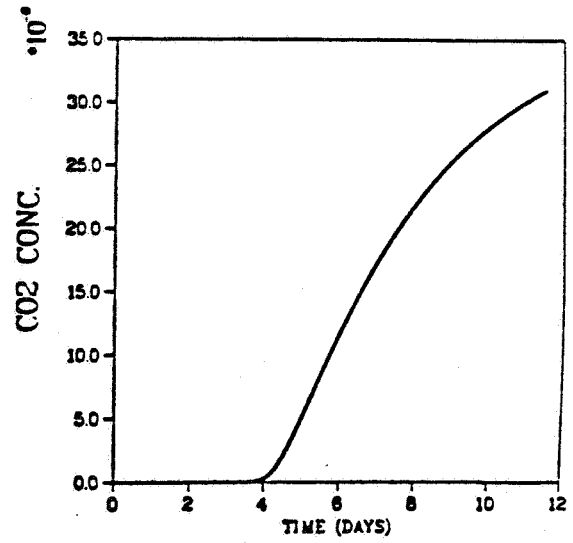
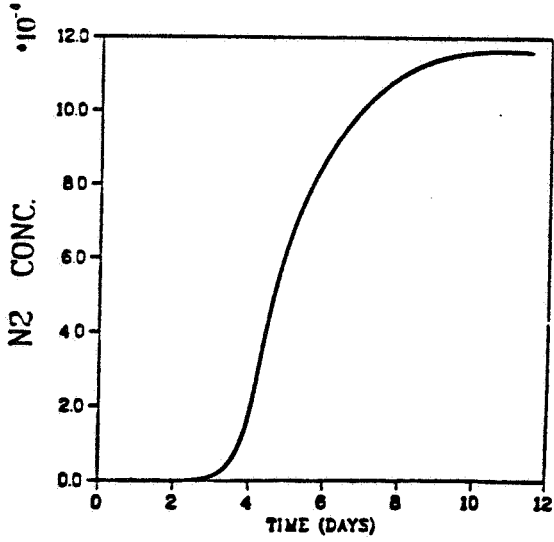
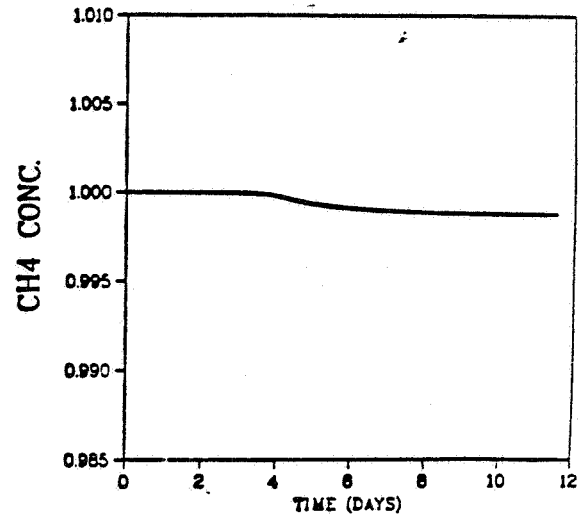
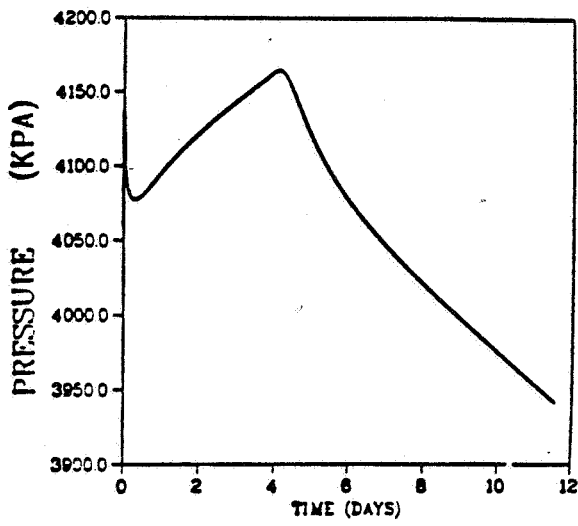
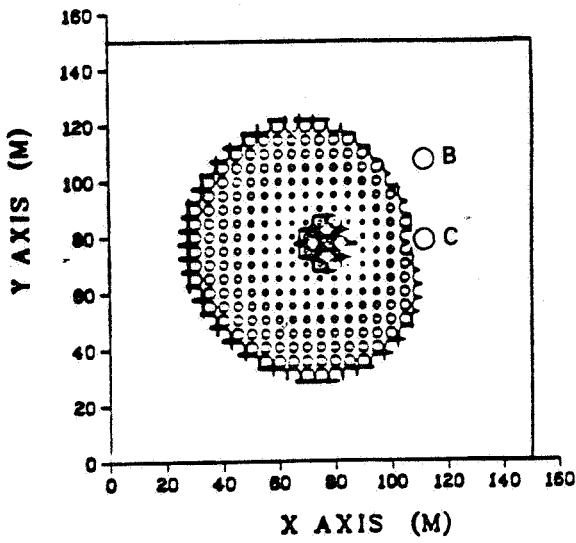
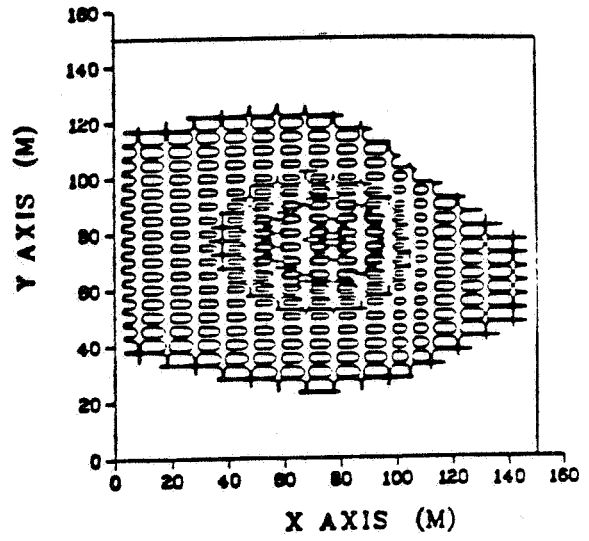


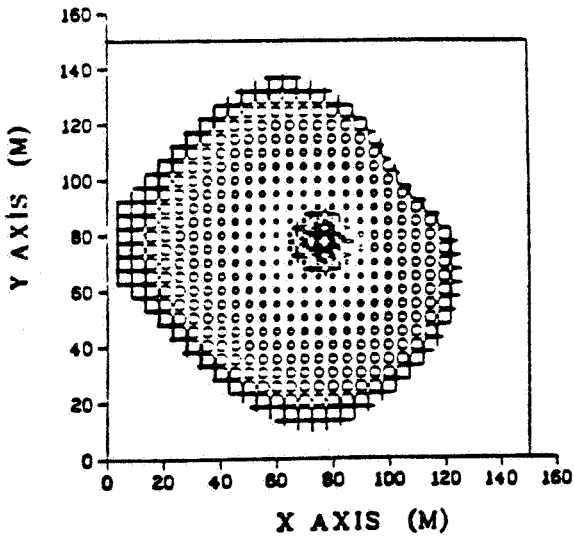
Figure B4. Pre-Test Simulations; Well C Pressure and Concentration-Time Histories for the Base Case



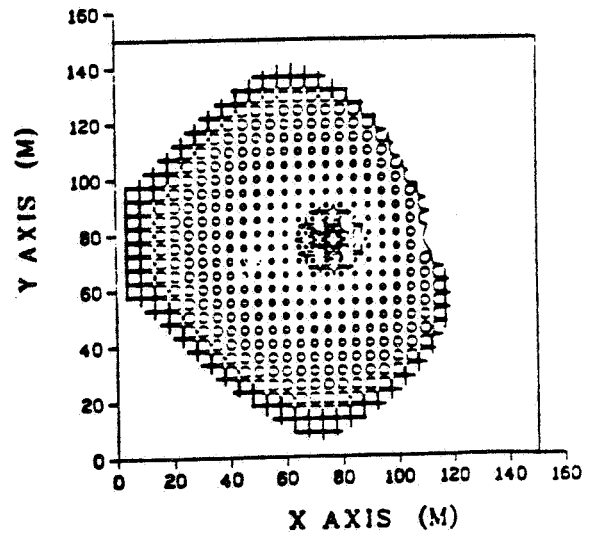
A.  $k_m \rightarrow 100 k_m$



B.  $L_x \rightarrow 4 L_x$

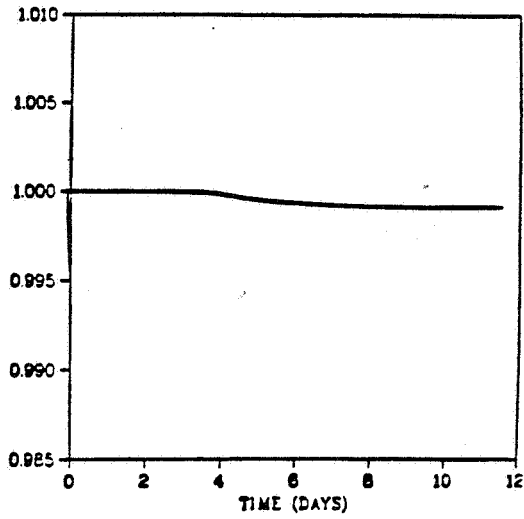


C. Explosive Fracture

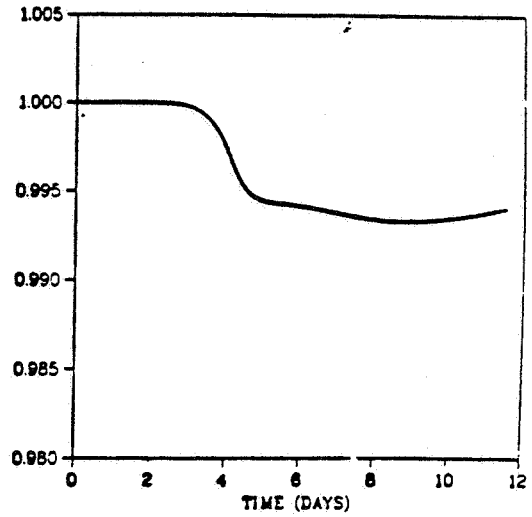


D. Well Springing

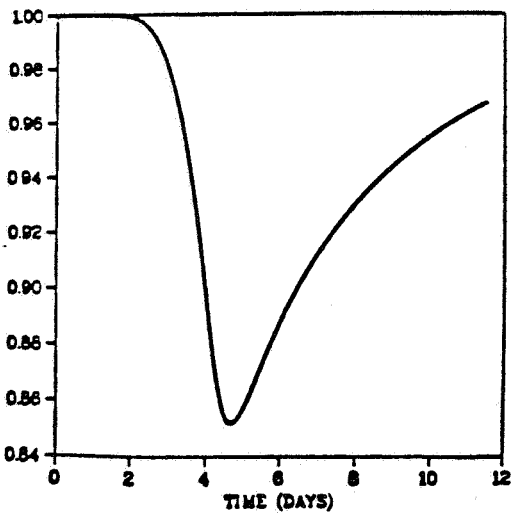
Figure B5. Pre-Test Simulations; Pressure Patterns for the 4 Variations at 4 Days



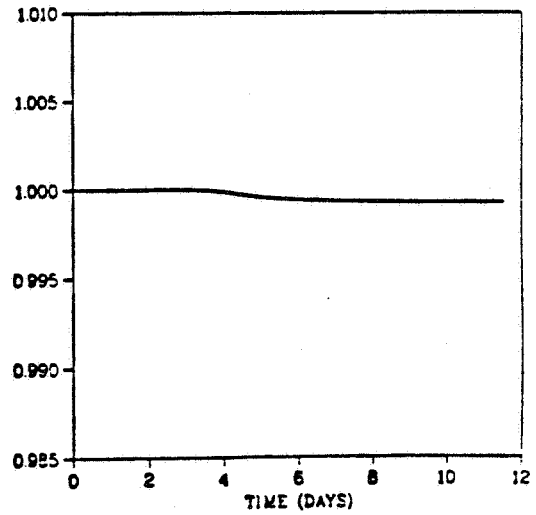
A.  $k_m \rightarrow 100 k_m$



B.  $L_x \rightarrow 4 L_x$

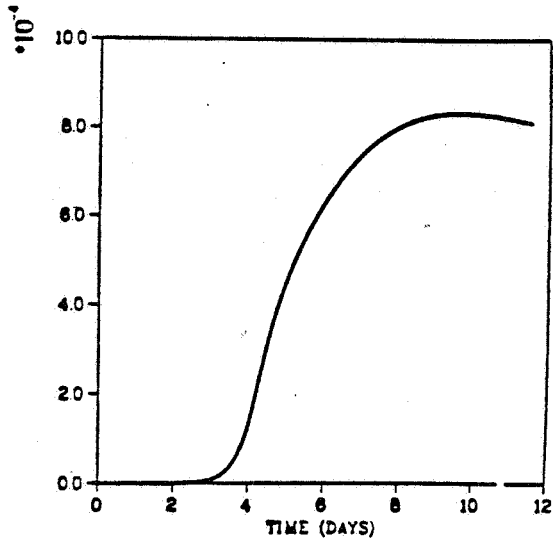


C. Explosive Fracture

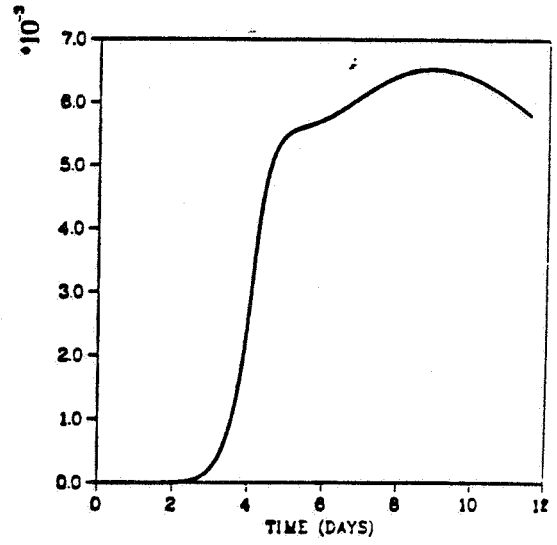


D. Well Springing

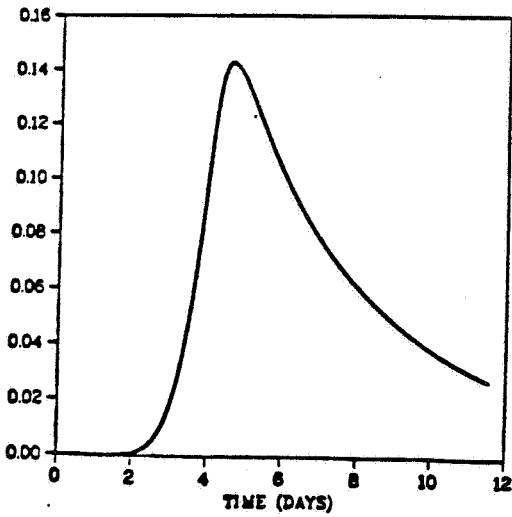
Figure B6. Pre-Test Simulations; Well C CH<sub>4</sub> Concentration-Time Histories for the 4 Variations



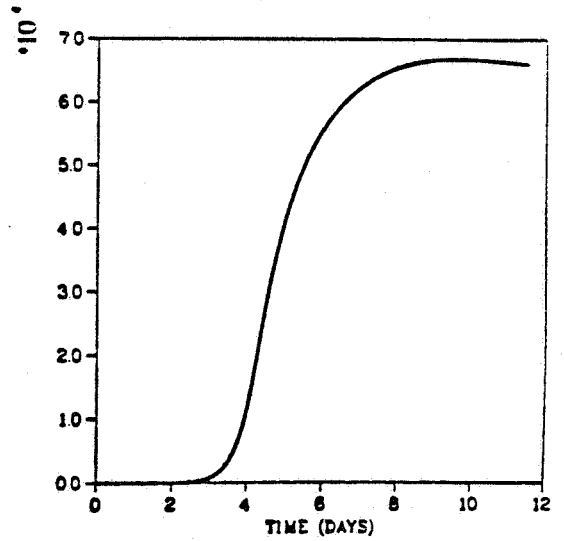
A.  $k_m \rightarrow 100 k_m$



B.  $L_x \rightarrow 4 L_x$

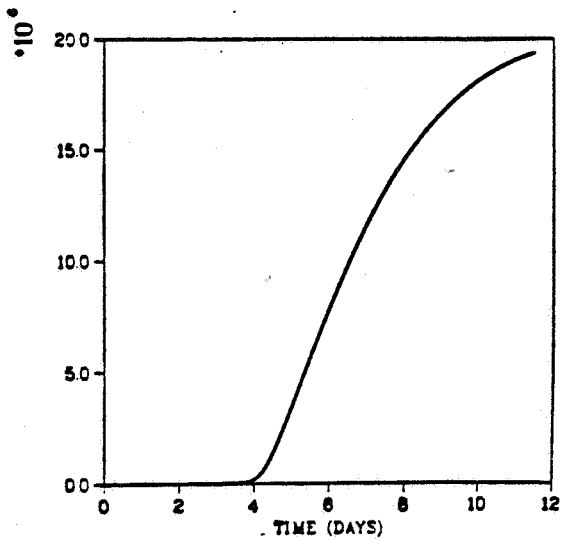


C. Explosive Fracture

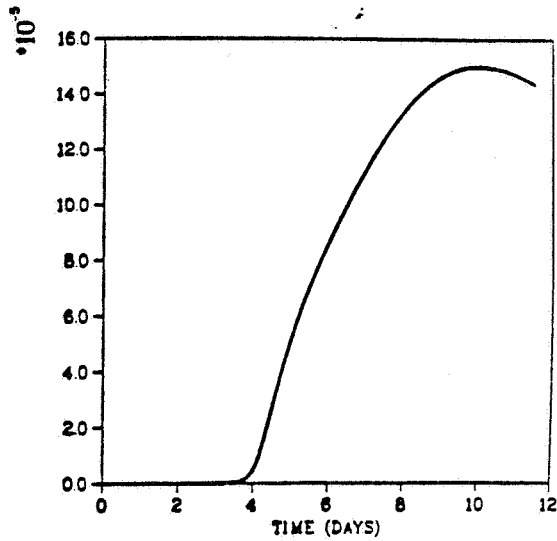


D. Well Springing

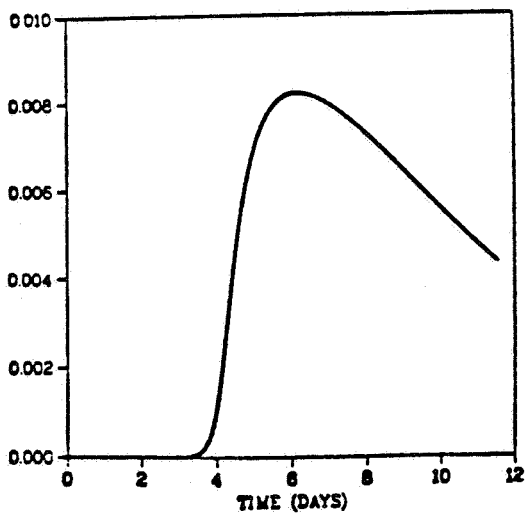
Figure B7. Pre-Test Simulations; Well C N<sub>2</sub> Concentration-Time Histories for the 4 Variations



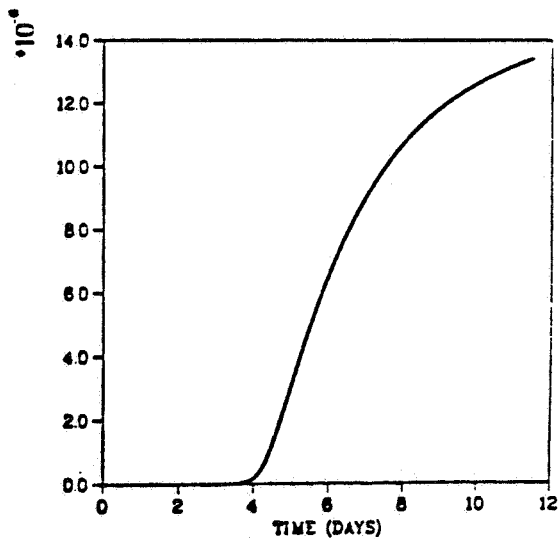
A.  $k_m \rightarrow 100 k_m$



B.  $L_x \rightarrow 4 L_x$



C. Explosive Fracture



D. Well Springing

Figure B8. Pre-Test Simulations; Well C CO<sub>2</sub> Concentration-Time Histories for the 4 Variations

APPENDIX C  
FIELD TEST DATA

date	time	a wellhead	a annulus	well a composition		
		press, psig	press, psig	% n2	% ch4	% c2h6
8/20	13:00	360.50	147.00			
8/20	14:00	359.00	150.40	2.08	74.45	8.17
8/20	14:20	633.50	157.70			
8/20	14:40	648.40	167.70			
8/20	15:00	636.50	177.60	93.18	0.00	0.00
8/20	15:30	646.80	192.70			
8/20	15:50	650.10	203.00			
8/20	16:10	652.10	213.70			
8/20	16:30	654.80	224.30			
8/20	16:50	656.80	235.10	91.82	0.00	0.00
8/20	17:10	655.20	246.00			
8/20	17:30	654.60	257.00			
8/20	17:50	628.20	267.70			
8/20	18:10	652.30	277.70			
8/20	18:30	649.50	289.80	91.46	0.00	0.00
8/20	18:50	652.20	301.20			
8/20	19:10	656.50	312.80			
8/20	19:30	659.30	324.60			
8/20	19:50	662.50	336.60			
8/20	20:10	665.40	348.90			
8/20	20:30	668.20	361.20			
8/20	20:50	669.10	373.60			
8/20	21:10	647.90	386.50			
8/20	21:30	648.70	399.10			
8/20	21:50	650.20	412.00	93.90	0.00	0.00
8/20	22:10	650.70	425.00			
8/20	22:30	651.80				
8/20	22:50	652.90				
8/20	23:10	653.30	465.10			
8/20	23:30	653.80	478.70	92.90	0.00	0.00
8/20	23:50	590.00	490.80			
8/21	00:10	218.30	481.60	88.92	.34	.03
8/21	00:30	195.80	455.40	86.78	3.54	.37
8/21	00:50	175.30	431.80	88.84	2.94	.31
8/21	01:10	152.50	409.40	90.90	3.29	.36

date	time	a wellhead		well a composition;		
		press, psig	a annulus press, psig	% n2	% ch4	% c2h6
8/21	01:30	137.00	389.30	91.18	3.54	.39
8/21	01:50	123.60	370.40			
8/21	02:10	112.30	353.90	89.70	3.87	.43
8/21	02:30	114.60	339.40	87.49	4.18	.48
8/21	02:50	101.90	323.70	90.70	4.11	.48
8/21	03:10	100.90	310.80	90.31	3.91	.44
8/21	03:30	81.90	305.70	86.42	5.29	.63
8/21	03:50	99.60	302.70			
8/21	04:10	110.20	300.60	82.31	10.36	1.23
8/21	04:30	96.00	298.90	79.40	12.07	1.43
8/21	04:50	93.80	297.00	76.11	13.99	1.63
8/21	05:10	106.70	294.70	75.51	14.72	.18
8/21	05:30	94.10	293.00	75.90	14.30	1.70
8/21	05:50	72.70	291.20			
8/21	06:10	76.20	288.90	74.45	16.49	.20
8/21	06:30	82.00	286.90			
8/21	06:50	89.70	285.30	74.56	15.74	1.86
8/21	07:10	92.60	283.40			
8/21	07:30	98.70	281.60	72.75	17.00	2.05
8/21	07:50	100.60	280.00			
8/21	08:10	103.50	278.40	71.29	18.29	2.15
8/21	08:30	108.90	276.80			
8/21	08:50	106.60	275.10			
8/21	09:10	97.20	273.90			
8/21	09:30	101.10	272.50	67.73	21.17	2.46
8/21	09:50	101.40	271.00			
8/21	10:10	105.70	269.60	66.73	22.03	2.54
8/21	10:30	97.30	267.80			
8/21	10:50	85.90	266.60			
8/21	11:10	390.90	410.80	63.97	24.31	2.80
8/21	11:30	120.20	263.80			
8/21	11:50	108.40	262.80	63.12	24.45	2.85
8/21	12:10	92.20	261.60			
8/21	12:30	85.90	260.30	59.03	27.96	3.22
8/21	12:50	95.60	259.30			
8/21	13:10	110.50	258.00	58.31	28.72	3.31
8/21	13:30	108.30	257.00			
8/21	13:50	106.20	255.70			
8/21	14:10	107.40	254.90	57.74	29.95	3.36
8/21	14:30	105.30	253.70			

date	time	a wellhead	a annulus	well a composition		
		press, psig	press, psig	% n2	% ch4	% c2h6
8/22	04:10	112.00	215.50			
8/22	04:30	110.80	214.70			
8/22	04:50	108.50	214.00	29.00	51.99	5.60
8/22	05:10	100.40	213.40			
8/22	05:30	98.20	212.50	27.80	53.09	5.69
8/22	06:10	90.90	211.10			
8/22	06:30	97.50	210.40	27.58	53.43	.57
8/22	06:50	100.40	209.60			
8/22	07:10	105.90	208.90	27.05	53.58	5.76
8/22	07:30	102.50	208.40			
8/22	07:50	102.20	207.60	26.57	53.72	.58
8/22	08:10	98.80	206.90			
8/22	08:30	99.30	206.10	25.13	55.13	5.92
8/22	08:50	96.00	205.40			
8/22	09:10	94.50	204.80			
8/22	09:30	99.30	203.90	25.05	55.93	5.96
8/22	09:50	100.30	203.00			
8/22	10:10	104.90	203.40	24.85	55.56	5.98
8/22	10:30	108.00	202.70			
8/22	10:50	107.30	202.40			
8/22	11:25	106.50	201.00			
8/22	11:45	104.50	200.90			
8/22	12:00	104.30	200.60	22.35	57.42	6.17
8/22	12:20	102.60	199.90			
8/22	12:40	103.10	199.10	22.39	57.96	6.25
8/22	13:00	99.50	198.80			
8/22	13:20	97.60	197.80			
8/22	13:40	100.70	197.50	21.42	59.10	6.21
8/22	14:00	98.30	196.70			
8/22	14:20	100.20	195.90	21.47	59.19	6.36
8/22	14:40	98.10	195.80			
8/22	15:00	96.20	195.10			
8/22	15:20	97.70	194.40	20.93	59.41	6.38
8/22	15:40	96.00	194.10			
8/22	16:00	98.00	193.40	21.01	59.92	6.30
8/22	16:20	96.80	192.80			
8/22	16:40	99.10	192.30	20.40	60.14	6.33
8/22	17:00	96.90	191.50			
8/22	17:20	99.00	191.00	19.80	59.75	6.27
8/22	17:40	96.90	190.50			

date	time	a wellhead	a annulus	well a composition :		
		press, psig	press, psig	% n2	% ch4	% c2h6
8/23	07:20	91.20	168.60	14.08	64.12	6.82
8/23	07:40	89.10	168.20			
8/23	08:00	87.40	167.60			
8/23	08:20	88.20	167.20			
8/23	08:35	87.00	166.90			
8/23	08:50	85.80	166.50			
8/23	09:20	91.60	164.80		63.55	6.87
8/23	09:40	92.40	164.70			
8/23	10:00	94.10	164.50			
8/23	10:20	100.00	164.20	13.93	63.69	6.89
8/23	10:40	102.20	163.90			
8/23	11:00	103.90	163.70			
8/23	11:20	109.80	163.10	13.11	63.72	6.82
8/23	11:40	108.10	163.00			
8/23	12:00	103.10	162.90			
8/23	12:20	101.50	162.40	14.15	74.92	8.15
8/23	12:40	99.70	161.90			
8/23	13:00	98.70	161.60			
8/23	13:20	102.10	161.50	13.41	69.47	7.47
8/23	13:40	102.00	161.00			
8/23	14:00	101.10	160.60			
8/23	14:20	104.50	160.20	14.40	76.07	8.06
8/23	14:40	103.50	160.10			
8/23	15:00	102.50	159.60			
8/23	15:20	106.00	159.30	12.74	68.82	7.43
8/23	15:40	105.00	159.10			
8/23	16:00	103.30	158.50			
8/23	16:20	106.30	158.30	13.64	74.99	8.01
8/23	16:40	103.50	157.90			
8/23	17:00	100.50	157.40			
8/23	17:20	100.70	157.20	12.33	71.68	7.61
8/23	17:40	97.50	156.80			
8/23	18:00	93.60	156.50			
8/23	18:20	89.60	155.90			
8/23	18:40	88.40	155.40			
8/23	19:00	94.20	155.00	12.83	71.09	7.54
8/23	19:20	96.00	154.50			
8/23	19:40	97.80	154.20			
8/23	20:00	103.50	153.80	13.42	73.51	8.00
8/23	20:20	105.30	153.40			

date	time	a wellhead	a annulus	well a composition		
		press, psig	press, psig	% n2	% ch4	% c2h6
8/24	10:20	89.60	140.50			
8/24	10:40	89.40	140.20			
8/24	11:00	87.50	140.10			
8/24	11:20	87.60	139.90			
8/24	11:40	91.40	139.70	9.50	66.64	7.04
8/24	12:00	91.60	139.90			
8/24	12:25	94.10	139.50	9.31	66.06	7.02
8/24	12:40	.40	139.20			
8/24	13:00	131.30	139.10			
8/24	13:20	122.60	139.00	8.96	66.72	7.10
8/24	13:55	100.40	138.60			
8/24	14:15	90.70	138.30			
8/24	14:40	98.70	138.10			
8/24	15:00	107.30	137.80			
8/24	15:20		137.20			
8/24	15:40	116.30	137.00	9.45	66.18	7.01
8/24	16:00	113.50	137.00			
8/24	16:20	109.50	136.70			
8/24	16:40	109.40	136.40	6.64	68.38	7.26
8/24	17:00	104.50	136.10			
8/24	17:20	100.00	135.90			
8/24	17:40	99.50	135.60	6.96	68.45	7.42
8/24	18:00	94.50	135.40			
8/24	18:20	89.00	135.10			
8/24	18:40	90.30	134.70	7.84	67.71	7.34
8/24	19:00	90.00	134.40			
8/24	19:20	92.70	134.10			
8/24	19:40	99.40	133.80	8.45	67.15	7.11
8/24	20:00	102.10	133.40			
8/24	20:20	104.80	133.10			
8/24	20:40	111.60	132.80	8.01	68.36	7.23
8/24	21:00	114.40	132.50			
8/24	21:20	112.20	133.00			
8/24	21:40	108.70	132.40	6.69	68.72	7.32
8/24	22:00	99.30	132.30			
8/24	22:20	97.50	132.30			
8/24	22:40	101.00	132.10	6.69	68.38	7.36
8/24	23:00	99.70	131.90			
8/24	23:20	98.40	131.10			
8/24	23:40	101.10	131.10	7.37	68.07	7.32

date	time	a wellhead	a annulus	well a composition		
		press, psig	press, psig	% n2	% ch4	% c2h6
8/25	13:20	104.60	124.40			
8/25	13:40	106.60	124.20			
8/25	14:00	106.90	124.00			
8/25	14:20	105.30	123.80			
8/25	14:40	107.90	123.80	5.19	70.12	7.59
8/25	15:00	104.00	123.80			
8/25	15:20	99.70	123.70			
8/25	15:40	99.60	123.50	5.08	70.00	7.57
8/25	16:00	95.40	123.20			
8/25	16:20	94.90	123.20			
8/25	16:40	99.70	122.90	5.94	69.71	7.37
8/25	17:00	101.30	122.70			
8/25	17:20	102.70	122.60			
8/25	17:40	103.90	122.30			
8/25	18:00	104.90	122.00			
8/25	19:20	107.40	121.30	4.63	70.27	7.47
8/25	19:40	99.60	121.10			
8/25	20:00	92.10	121.00			
8/25	20:20	96.40	120.70	4.69	70.63	7.72
8/25	20:40	96.60	120.60			
8/25	21:00	96.80	120.40			
8/25	21:40	102.20	120.10	5.72	68.43	7.25
8/25	22:00	102.60	119.80			
8/25	22:20	102.80	119.60			
8/25	22:40	105.60	119.60	5.05	69.20	7.55
8/25	23:00	102.00	119.40			
8/25	23:20	98.50	119.20			
8/25	23:40	99.00	119.00	4.39	69.69	7.52
8/26	00:00	95.30	118.80			
8/26	00:20	91.70	118.70			
8/26	00:40	93.90	118.40	5.13	69.42	7.54
8/26	01:00	92.10	118.30			
8/26	01:20	92.20	118.00			
8/26	01:40	97.00	117.90	5.63	68.29	7.35
8/26	02:00	97.50	117.70			
8/26	02:20	98.20	117.50			
8/26	02:40	102.90	117.40	5.40	69.31	7.53
8/26	03:00	103.60	117.30			
8/26	03:20	103.90	117.20			
8/26	04:00	103.00	117.00	4.05	70.24	7.65

date	time	a		well a composition		
		wellhead press, psig	annulus press, psig	% n2	% ch4	% c2h6
8/26	18:20	99.80	112.80			
8/26	18:40	98.30	112.50			

date	time	b wellhead press, psig	well b composition		
			% n2	% ch4	% c2h6
8/21	01:30	103.10			
8/21	01:50	103.10			
8/21	02:10	103.50			
8/21	02:30	103.60			
8/21	02:50	103.50			
8/21	03:10	103.70			
8/21	03:30	103.70			
8/21	03:50	103.70			
8/21	04:10	103.80			
8/21	04:30	104.00			
8/21	04:50	104.10			
8/21	05:10	103.90			
8/21	05:30	104.00			
8/21	05:50	104.10			
8/21	06:10	104.00			
8/21	06:30	103.90			
8/21	06:50	104.10			
8/21	07:10	104.10			
8/21	07:30	104.00			
8/21	07:50	104.10			
8/21	08:10	104.20			
8/21	08:30	104.10			
8/21	08:50	104.50	2.13	74.48	8.16
8/21	09:10	104.50			
8/21	09:30	104.50			
8/21	09:50	104.30			
8/21	10:10	104.20			
8/21	10:30	103.80			
8/21	10:50	104.40	2.13	74.33	8.04
8/21	11:10	256.70			
8/21	11:30	104.00			
8/21	11:50	104.00			
8/21	12:10	103.80			
8/21	12:30	103.70			
8/21	12:50	103.60			
8/21	13:10	103.60			
8/21	13:30	103.60			
8/21	13:50	104.00	2.12	74.34	8.05
8/21	14:10	103.80			
8/21	14:30	103.70			

date	time	b wellhead press, psig	well b composition		
			% n2	% ch4	% c2h6
8/22	04:10	107.60	2.12	74.09	7.94
8/22	04:30	107.60			
8/22	04:50	107.60			
8/22	05:10	107.80			
8/22	05:30	107.70			
8/22	06:10	108.40			
8/22	06:30	108.40			
8/22	06:50	108.40			
8/22	07:10	108.40			
8/22	07:30	108.70			
8/22	07:50	108.60			
8/22	08:10	108.80			
8/22	08:30	108.70			
8/22	08:50	109.20	2.12	73.46	7.88
8/22	09:10	109.10			
8/22	09:30	108.90			
8/22	09:50	108.60			
8/22	10:10	109.30			
8/22	10:30	109.40	2.14	74.38	7.89
8/22	10:50	109.80			
8/22	11:25	109.90			
8/22	11:45	110.00			
8/22	12:00	110.00			
8/22	12:20	110.20			
8/22	12:40	110.30			
8/22	13:00	110.40			
8/22	13:20	111.10	2.10	73.27	7.84
8/22	13:40	110.80			
8/22	14:00	110.60			
8/22	14:20	110.70			
8/22	14:40	110.50			
8/22	15:00	110.80	2.16	75.03	7.93
8/22	15:20	111.00			
8/22	15:40	111.00			
8/22	16:00	110.70			
8/22	16:20	110.90			
8/22	16:40	110.90			
8/22	17:00	110.80			
8/22	17:20	111.00			
8/22	17:40	111.00			

date	time	b wellhead press, psig	well b composition		
			% n2	% ch4	% c2h6
8/23	07:20	117.10			
8/23	07:40	117.10			
8/23	08:00	117.40	22.89	57.36	6.37
8/23	08:20	117.30			
8/23	08:35	117.40			
8/23	08:50	117.70			
8/23	09:20	116.90			
8/23	09:40	116.90			
8/23	10:00	117.50	23.25	64.66	7.00
8/23	10:20	117.40			
8/23	10:40	117.50			
8/23	11:00	118.10	23.04	68.70	7.46
8/23	11:20	117.90			
8/23	11:40	118.20			
8/23	12:00	118.30	20.19	64.75	7.05
8/23	12:20	118.60			
8/23	12:40	118.50			
8/23	13:00	118.90	20.12	71.17	4.06
8/23	13:20	119.20			
8/23	13:40	119.00			
8/23	14:00	119.10	17.23	66.52	7.23
8/23	14:20	119.30			
8/23	14:40	118.90			
8/23	15:00	119.40	16.49	70.75	7.61
8/23	15:20	119.10			
8/23	15:40	119.40			
8/23	16:00	119.40	14.72	69.81	7.70
8/23	16:20	119.60			
8/23	16:40	119.40			
8/23	17:00	119.80	13.58	70.87	7.78
8/23	17:20	120.00			
8/23	17:40	119.90			
8/23	18:00	120.20	12.45	69.50	7.38
8/23	18:20	120.20			
8/23	18:40	120.50	10.83	65.58	6.97
8/23	19:00	120.50			
8/23	19:20	120.50			
8/23	19:40	120.90	10.24	66.95	7.21
8/23	20:00	120.90			
8/23	20:20	120.70			

date	time	b wellhead press, psig	well b composition		
			% n2	% ch4	% c2h6
8/24	10:20	124.60	5.13	69.26	7.42
8/24	10:40	124.60			
8/24	11:00	124.40			
8/24	11:20	124.90	5.02	69.95	7.44
8/24	11:40	124.90			
8/24	12:00	125.10			
8/24	12:25	125.20			
8/24	12:40	125.50	4.81	70.25	7.53
8/24	13:00	125.40			
8/24	13:20	125.50			
8/24	13:55	125.10			
8/24	14:15				
8/24	14:40	125.60			
8/24	15:00	126.30	4.56	70.68	7.52
8/24	15:20	126.00			
8/24	15:40	126.10			
8/24	16:00	126.50	4.44	70.15	7.44
8/24	16:20	126.30			
8/24	16:40	126.20			
8/24	17:00	126.40	4.38	70.73	7.65
8/24	17:20	126.60			
8/24	17:40	126.50			
8/24	18:00	126.60	4.28	70.34	7.50
8/24	18:20	126.60			
8/24	18:40	126.60			
8/24	19:00	126.70	4.20	70.37	7.61
8/24	19:20	126.60			
8/24	19:40	126.50			
8/24	20:00	126.50	4.16	71.21	7.55
8/24	20:20	126.30			
8/24	20:40	126.10			
8/24	21:00	126.30	4.12	71.89	7.84
8/24	21:20	127.30			
8/24	21:40	126.70			
8/24	22:00	127.40	3.99	71.22	7.65
8/24	22:20	127.70			
8/24	22:40	127.70			
8/24	23:00	128.10	3.92	70.56	7.48
8/24	23:20	127.10			
8/24	23:40	127.40			

date	time	b wellhead press, psig	well b composition		
			% n2	% ch4	% c2h6
8/25	13:20	128.50			
8/25	13:40	128.50			
8/25	14:00	128.30	3.19	70.99	7.60
8/25	14:20	128.00			
8/25	14:40	127.80			
8/25	15:00	128.10	3.20	72.14	7.87
8/25	15:20	128.10			
8/25	15:40	128.00			
8/25	16:00	128.20	3.18	72.09	7.74
8/25	16:20	128.10			
8/25	16:40	128.00			
8/25	17:00	128.10			
8/25	17:20	128.00			
8/25	17:40	127.90	3.10	71.53	7.57
8/25	18:00	127.70			
8/25	19:20	127.50			
8/25	19:40	127.60	3.07	71.99	7.84
8/25	20:00	127.80			
8/25	20:20	127.70			
8/25	20:40	127.80	3.03	70.99	7.66
8/25	21:00	127.80			
8/25	21:40	127.80			
8/25	22:00	128.00	2.99	71.41	7.78
8/25	22:20	127.70			
8/25	22:40	127.80			
8/25	23:00	128.00	2.95	71.16	7.73
8/25	23:20	128.00			
8/25	23:40	127.90			
8/26	00:00	128.00	2.90	70.46	7.59
8/26	00:20	128.10			
8/26	00:40	127.90			
8/26	01:00	128.30	2.92	70.92	7.53
8/26	01:20	128.10			
8/26	01:40	127.90			
8/26	02:00	128.30	2.89	71.55	7.77
8/26	02:20	128.00			
8/26	02:40	128.00			
8/26	03:00	128.30	2.85	70.81	7.63
8/26	03:20	128.20			
8/26	04:00	128.10			

date	time	b wellhead	well b composition		
		press, psig	% n2	% ch4	% c2h6
8/26	18:20	127.20			
8/26	18:40	126.90			

date	time	c wellhead press, psig	well c composition		
			% n2	% ch4	% c2h6
8/21	01:30	509.00			
8/21	01:50	507.00	2.61	74.57	8.03
8/21	02:10	504.10			
8/21	02:30	501.10			
8/21	02:50	498.40			
8/21	03:10	495.60			
8/21	03:30	493.00			
8/21	03:50	491.30	10.89	67.97	7.52
8/21	04:10	488.60			
8/21	04:30	486.10			
8/21	04:50	483.50			
8/21	05:10	481.10			
8/21	05:30	479.40			
8/21	05:50	478.30	11.17	69.18	7.45
8/21	06:10	475.30			
8/21	06:30	474.80	5.21	73.24	7.68
8/21	06:50	473.20			
8/21	07:10	473.00	11.03	67.92	7.47
8/21	07:30	470.30			
8/21	07:50	470.40	26.05	55.05	6.96
8/21	08:10	467.50			
8/21	08:30	466.20	32.09	49.22	5.69
8/21	08:50	462.20			
8/21	09:10	460.60	38.42	43.78	4.91
8/21	09:30	457.50			
8/21	09:50	456.60	38.99	44.85	4.89
8/21	10:10	453.80			
8/21	10:30	452.50	3.04	76.54	6.81
8/21	10:50	450.90			
8/21	11:10	450.30			
8/21	11:30	450.70	2.21	76.75	7.92
8/21	11:50	449.60			
8/21	12:10	449.80	2.19	76.39	7.88
8/21	12:30	448.80			
8/21	12:50	449.00	2.17	75.89	7.85
8/21	13:10	448.00			
8/21	13:30	448.50	2.17	75.76	7.83
8/21	13:50	447.20			
8/21	14:10	446.40			
8/21	14:30	446.80	2.15	75.47	7.94

date	time	c wellhead press, psig	well c composition		
			% n2	% ch4	% c2h6
8/22	04:10	422.60			
8/22	04:30	423.10	2.16	74.65	7.62
8/22	04:50	422.00			
8/22	05:10	422.60	2.16	75.09	7.53
8/22	05:30	421.40			
8/22	06:10	420.80	2.11	73.58	7.54
8/22	06:30	419.70			
8/22	06:50	420.20	2.15	74.72	7.67
8/22	07:10	419.20			
8/22	07:30	419.30	2.10	73.66	7.53
8/22	07:50	418.30			
8/22	08:10	419.10	2.17	75.25	7.63
8/22	08:30	418.10			
8/22	08:50	417.20			
8/22	09:10	418.00	2.13	75.11	7.75
8/22	09:30	417.30			
8/22	09:50	418.10	2.17	75.98	7.81
8/22	10:10	411.90			
8/22	10:30	411.20			
8/22	10:50	411.80	2.12	74.91	7.84
8/22	11:25	410.60			
8/22	11:45	409.70			
8/22	12:00	409.00			
8/22	12:20	409.90	2.12	75.13	7.73
8/22	12:40	409.60			
8/22	13:00	410.40	2.13	75.23	7.74
8/22	13:20	409.50			
8/22	13:40	408.60			
8/22	14:00	409.50	2.12	75.61	7.83
8/22	14:20	408.10			
8/22	14:40	409.30	2.13	75.59	7.80
8/22	15:00	408.10			
8/22	15:20	406.90			
8/22	15:40	408.70	2.11	75.54	7.82
8/22	16:00	405.10			
8/22	16:20	405.50	2.08	75.09	7.97
8/22	16:40	400.90			
8/22	17:00	399.50	2.11	75.71	7.92
8/22	17:20	394.90			
8/22	17:40	393.40	2.11	75.59	7.93

date	time	c wellhead press, psig	well c composition		
			% n2	% ch4	% c2h6
8/23	07:20	390.60			
8/23	07:40	392.20	27.65	54.43	5.91
8/23	08:00	391.10			
8/23	08:20	391.10			
8/23	08:35	392.90			
8/23	08:50	391.80			
8/23	09:20	391.00			
8/23	09:40	393.20	27.22	53.78	5.91
8/23	10:00	392.80			
8/23	10:20	394.20			
8/23	10:40	395.50	26.96	52.81	5.77
8/23	11:00	393.70			
8/23	11:20	393.50			
8/23	11:40	394.10	24.55	65.41	6.80
8/23	12:00	393.90			
8/23	12:20	394.30			
8/23	12:40	395.90	26.01	61.76	6.71
8/23	13:00	394.30			
8/23	13:20	395.10			
8/23	13:40	394.90	24.52	60.98	6.79
8/23	14:00	395.10			
8/23	14:20	394.30			
8/23	14:40	391.90	23.53	56.65	6.09
8/23	15:00	388.20			
8/23	15:20	385.60			
8/23	15:40	384.40	19.32	66.06	7.05
8/23	16:00	381.30			
8/23	16:20	380.40			
8/23	16:40	379.20	16.25	62.70	6.68
8/23	17:00	376.50			
8/23	17:20	373.90			
8/23	17:40	374.90	16.07	68.75	7.32
8/23	18:00	370.90			
8/23	18:20	368.20			
8/23	18:40	368.90			
8/23	19:00	368.60			
8/23	19:20	371.70	13.75	65.04	6.95
8/23	19:40	372.00			
8/23	20:00	369.90			
8/23	20:20	367.90	14.19	63.57	6.92

date	time	c wellhead press, psig	well c composition		
			% n2	% ch4	% c2h6
8/24	10:20	388.30			
8/24	10:40	387.80			
8/24	11:00	388.70	13.38	63.88	6.85
8/24	11:20	389.10			
8/24	11:40	387.80			
8/24	12:00	389.30	11.73	65.77	6.98
8/24	12:25	388.70			
8/24	12:40	388.70			
8/24	13:00	390.10	14.17	63.35	6.93
8/24	13:20	389.50			
8/24	13:55	389.20			
8/24	14:15	388.50			
8/24	14:40	389.10			
8/24	15:00	388.60			
8/24	15:20	389.00	11.36	65.92	6.93
8/24	15:40	387.10			
8/24	16:00	384.20			
8/24	16:20	382.30	9.57	67.25	7.33
8/24	16:40	379.40			
8/24	17:00	376.20			
8/24	17:20	375.00	8.79	67.35	7.20
8/24	17:40	371.90			
8/24	18:00	368.90			
8/24	18:20	367.70	7.74	68.34	7.28
8/24	18:40	367.60			
8/24	19:00	368.40			
8/24	19:20	369.40	7.97	68.56	7.33
8/24	19:40	366.10			
8/24	20:00	363.20			
8/24	20:20	362.10	7.94	69.35	7.40
8/24	20:40	359.10			
8/24	21:00	356.70			
8/24	21:20	359.00	10.03	66.01	7.09
8/24	21:40	359.10			
8/24	22:00	360.30			
8/24	22:20	363.00	10.33	66.72	7.23
8/24	22:40	363.20			
8/24	23:00	363.90			
8/24	23:20	366.00	10.62	66.67	7.19
8/24	23:40	366.00			

date	time	c wellhead press, psig	well c composition		
			% n2	% ch4	% c2h6
8/25	13:20	380.30			
8/25	13:40	380.30			
8/25	14:00	380.10			
8/25	14:20	381.20	8.46	68.39	7.44
8/25	14:40	380.80			
8/25	15:00	378.40			
8/25	15:20	376.50	7.12	69.28	7.55
8/25	15:40	373.50			
8/25	16:00	371.80			
8/25	16:20	370.60	7.50	68.99	7.59
8/25	16:40	367.60			
8/25	17:00	365.20			
8/25	17:20	362.70			
8/25	17:40	360.00			
8/25	18:00	358.40	5.82	70.56	7.58
8/25	19:20	354.60			
8/25	19:40	355.60			
8/25	20:00	357.90	6.98	69.11	7.45
8/25	20:20	358.50			
8/25	20:40	359.20			
8/25	21:00	361.00	7.34	69.43	7.62
8/25	21:40	358.30			
8/25	22:00	356.10			
8/25	22:20	358.40	7.88	67.41	7.38
8/25	22:40	359.10			
8/25	23:00	359.80			
8/25	23:20	361.60	8.35	66.25	7.20
8/25	23:40	362.00			
8/26	00:00	362.40			
8/26	00:20	364.10	8.78	67.75	7.42
8/26	00:40	364.30			
8/26	01:00	364.80			
8/26	01:20	365.70	9.20	67.34	7.37
8/26	01:40	363.10			
8/26	02:00	363.90			
8/26	02:20	365.50	9.80	65.87	7.18
8/26	02:40	365.80			
8/26	03:00	366.10			
8/26	03:20	367.60	10.02	66.66	7.27
8/26	04:00	368.00			

date	time	c wellhead	well c composition		
		press, psig	% n2	% ch4	% c2h6
8/26	18:20	94.80			
8/26	18:40	92.80			

<u>Date</u>	<u>Time</u>	<u>Pressure, psig</u>	<u>Date</u>	<u>Time</u>	<u>Pressure, psig</u>
08/19/81	14:11	364.00	08/21/81	00:21	254.52
	14:56	368.41		00:56	208.18
	16:56	375.93		01:56	145.11
	17:11	376.31		02:26	123.31
	20:56	390.52		02:41	135.24
	21:11	391.13		02:56	121.41
	22:56	392.27		03:06	117.23
08/20/81	00:56	392.87		03:11	120.04
	02:56	393.25		03:26	97.25
	04:56	393.79		04:41	130.68
	06:56	394.24		04:56	104.16
	05:56	394.85		05:11	124.45
	10:41	395.76	<u>Well</u>	06:06	81.98
	10:56	396.60	<u>A</u>	06:56	103.33
	11:26	397.36	<u>Data</u>	07:56	116.17
	12:56	399.64		08:06	119.28
	13:26	393.48		08:26	119.28
	13:46	394.17		08:46	125.44
	14:06	394.17		08:56	125.44
	14:26	459.66		09:11	109.41
	14:41	694.69		09:16	115.56
	14:46	713.52		09:56	116.09
	14:51	719.01		10:16	120.88
	14:56	729.00		10:46	110.55
	15:06	714.29		10:56	98.35
	15:11	721.60		11:06	143.75
	15:46	723.89		11:11	143.75
	16:11	728.16		12:41	98.01
	16:56	733.34		12:51	98.01
	17:11	735.63		13:11	124.75
	17:26	732.73		13:56	120.19
	17:41	732.58		14:56	120.35
	17:56	719.62		16:56	110.17
	18:11	681.35		17:56	109.48
	18:16	705.14		18:26	120.12
	18:26	708.95		18:56	112.60
	18:41	735.17		19:26	111.46
	18:46	741.96		20:56	117.99
	18:51	728.16		21:11	122.09
	18:56	728.54		22:56	118.52
	19:56	742.11	08/22/81	00:56	115.48
	20:56	752.10		02:11	108.04
	21:11	753.85		02:56	114.42
	21:26	730.29		04:11	128.40
	21:56	731.82		04:56	126.50
	22:56	735.63		06:26	104.85
	23:41	736.39		07:11	120.65
	23:56	695.99		09:11	107.13

<u>Date</u>	<u>Time</u>	<u>Pressure, psig</u>	<u>Date</u>	<u>Time</u>	<u>Pressure, psig</u>
08/24/81	22:30	113.13	08/25/81	22:30	117.76
	22:50	116.32		22:55	120.88
	23:10	115.64		23:45	113.74
	23:30	114.12		23:55	113.89
	23:45	116.24			
08/25/81	00:30	114.19	08/26/81	00:30	106.21
	00:55	116.47		00:55	107.89
	01:30	113.96		01:10	106.52
	01:45	116.24		01:15	106.59
	02:45	113.81		01:45	111.91
	02:55	115.71		02:30	113.20
	03:30	113.13		02:55	119.05
	03:45	115.10		03:30	119.89
	04:30	112.37		03:45	121.41
	04:55	114.12		04:00	119.05
	05:10	112.52		04:10	119.05
	05:30	112.44		04:55	111.61
	06:15	118.90		05:00	111.61
	07:15	114.65	<u>Well</u>	05:10	113.28
	07:30	115.71	<u>A</u>	06:00	113.20
	08:30	113.28	<u>Data</u>	06:15	116.85
	08:55	116.55		07:00	116.85
	09:30	115.56		07:10	120.42
	09:45	116.67		07:50	112.60
	10:30	118.45		08:15	113.96
	10:55	121.03		09:00	112.67
	11:30	112.60		09:10	116.32
	11:50	112.67		10:45	117.08
	12:45	109.63		10:55	121.26
	12:55	115.33		11:10	121.03
	14:00	121.33		11:30	116.09
	14:30	118.90		11:45	115.71
	14:55	121.26		12:10	110.47
	15:30	112.44		12:30	110.24
	15:45	112.29		12:55	113.74
	16:15	106.90		13:10	118.75
	16:30	106.90		14:15	108.65
	16:50	111.99		14:45	108.80
	18:15	118.52		15:00	103.78
	18:55	123.84		15:15	102.95
	19:15	123.84		15:30	102.95
	19:20	122.93		16:00	108.34
	20:15	105.68		16:50	111.76
	20:30	110.17		16:55	112.60
	21:10	110.85		17:20	114.34
	21:20	114.80		18:00	119.13
	21:45	115.33		18:45	111.99
	22:00	117.54		19:00	111.08
				19:15	106.44

Date	Time	Pressure, psig	Date	Time	Pressure, psig
08/30/81	09:00	369.78	08/20/81	10:30	93.91
	11:00	370.46		11:30	95.69
<hr/>				13:00	96.14
Well No. 10056-B				14:45	97.46
<hr/>				15:30	98.48
Date	Time	Pressure, psig		16:30	99.54
08/17/81	14:30	1.47		17:30	100.51
	15:30	2.99		18:30	101.93
	16:30	4.92		19:15	102.18
	17:30	7.06		19:30	102.99
	18:30	8.78		20:30	104.06
	19:30	11.07		22:30	106.14
	20:30	13.15	08/21/81	00:30	107.21
	22:30	17.01		02:30	108.07
08/18/81	00:30	20.61		04:30	108.38
	02:30	23.96		06:30	108.63
	04:30	27.41		08:30	108.63
	06:30	30.46		10:30	108.53
	08:30	33.60		12:30	108.53
	10:30	35.89		14:30	108.12
	12:30	38.38		16:30	108.17
	14:30	40.61		18:30	108.68
	16:30	42.69		19:30	109.29
	18:30	44.62		20:30	109.80
	20:30	46.40		22:30	110.30
	22:30	48.17	08/22/81	00:30	111.17
08/19/81	00:30	49.39		02:30	112.18
	02:30	50.76		04:15	112.18
	04:30	52.18		04:30	113.05
	06:30	53.20		06:30	113.50
	07:30	53.30		06:50	113.60
	08:30	51.68		07:00	114.06
	10:30	49.64		08:30	114.06
	12:30	47.82		10:30	114.87
	14:30	51.17		11:30	114.87
	16:30	55.28		12:30	115.74
	18:30	59.90		13:15	116.24
	20:30	64.47		14:30	116.29
	22:30	68.48		15:45	116.29
08/20/81	00:30	72.94		16:30	116.85
	02:30	77.41		18:30	117.41
	04:30	81.73		20:30	117.82
	06:30	85.79		22:30	118.78
	08:30	90.20	08/23/81	00:30	119.39
<hr/>				02:30	120.56
				04:30	121.68

<u>Date</u>	<u>Time</u>	<u>Pressure, psig</u>	
08/30/81	04:31	198.38	
	06:31	199.70	
	08:31	200.96	
	10:31	202.39	
	12:31	203.65	
	14:31	204.77	
	16:31	205.69	
	18:31	206.95	<u>Well</u>
	20:31	208.12	<u>B</u>
	21:41	208.58	
	22:31	209.14	<u>Data</u>
08/31/81	00:31	210.20	
	02:31	211.22	
	04:31	212.13	
	06:31	213.15	
	08:31	214.11	
	10:31	215.03	
	11:01	215.22	
	11:05	201.00 (WHP)	